

Degradation at the InSight Landing Site, Homestead Hollow, Mars: Constraints from Rock Heights and Shapes

John A. Grant¹, Sharon A Wilson¹, Matthew P. Golombek², Allyson R. Trussell³, Nicholas Hale Warner⁴, Nathan Robert Williams⁵, Catherine M. Weitz⁶, Hallie Gengl⁷, and Robert G Deen⁷

¹Smithsonian Institution

²California Institute of Technology/JPL

³California Institute of Technology

⁴SUNY Geneseo

⁵Jet Propulsion Lab

⁶Planetary Science Institute

⁷Jet Propulsion Laboratory

November 24, 2022

Abstract

Rock heights and three-dimensional shapes around the InSight lander in Homestead hollow, Mars, provide new constraints on modification of the degraded 27 m in diameter impact crater and are a tool for characterizing degradation on regolith-covered lava plains on Mars. Decreasing average rock height and increasing percentage of fragments where height comprises the short axis from outside to within the hollow supports significant ejecta deflation accompanied by infilling of the interior. Rock relief outside the hollow is compared with expectations of pristine ejecta thickness and indicates up to ~40 cm of near-rim early deflation (decreasing to a few cm out to one diameter) can account for the predicted eolian component of infilling and that other eolian infilling sources are not required. Scattered rocks in the hollow are ejecta from subsequent nearby impacts and their mostly buried expression is consistent with subsequent long-term degradation estimated to be 10-4 m/Myr. Basalt rock shapes at InSight are likely similar to basalt rock shapes on Earth, but appear more platy, bladed, and elongate in a triangular form factor plot and more discoidal and bladed in an axes ratio plot. Nevertheless, addition of 10 cm to near rim rock heights to account for continued partial embedding in ejecta would result in rock shapes quite similar to terrestrial rocks. Consistency between degradation estimates based on current rock relief and rock shape after accounting for partial embedding in ejecta indicates up to ~30-40 cm early (~0.1 Ga) near-rim deflation was followed by much lesser long-term degradation.

Degradation at the *InSight* Landing Site, *Homestead Hollow*, Mars: Constraints from Rock Heights and Shapes

J. A. Grant¹, S. A. Wilson¹, M. Golombek², A. Trussell^{2,3}, N. H. Warner⁴, N. Williams², C. M. Weitz⁵, H. Abarca², R. Deen²

¹Center for Earth and Planetary Studies, National Air and Space Museum, Smithsonian Institution, 6th at Independence SW, Washington, DC, 20560 ORCID: <https://orcid.org/0000-0001-8276-1281>

²Jet Propulsion Laboratory, California Institute of Technology, Pasadena, CA,

³California Institute of Technology, Pasadena, CA,

⁴SUNY Geneseo, Department of Geological Sciences, 1 College Circle, Geneseo, NY 14454

Submitted to Earth and Space Science 7/29/21

Abstract: Rock heights and three-dimensional shapes around the *InSight* lander in *Homestead hollow*, Mars, provide new constraints on modification of the degraded 27 m in diameter impact crater and are a tool for characterizing degradation on regolith-covered lava plains on Mars. Decreasing average rock height and increasing percentage of fragments where height comprises the short axis from outside to within the hollow supports significant ejecta deflation accompanied by infilling of the interior. Rock relief outside the hollow is compared with expectations of pristine ejecta thickness and indicates up to ~40 cm of near-rim early deflation (decreasing to a few cm out to one diameter) can account for the predicted eolian component of infilling and that other eolian infilling sources are not required. Scattered rocks in the hollow are ejecta from subsequent nearby impacts and their mostly buried expression is consistent with subsequent long-term degradation estimated to be 10^{-4} m/Myr. Basalt rock shapes at *InSight* are likely similar to basalt rock shapes on Earth, but appear more platy, bladed, and elongate in a triangular form factor plot and more discoidal and bladed in an axes ratio plot. Nevertheless, addition of 10 cm to near rim rock heights to account for continued partial embedding in ejecta would result in rock shapes quite similar to terrestrial rocks. Consistency between degradation estimates based on current rock relief and rock shape after accounting for partial embedding in ejecta indicates up to ~30-40 cm early (~0.1 Ga) near-rim deflation was followed by much lesser long-term degradation.

Key Points

Rock heights and shapes at *Homestead hollow* indicate early transport of deflated ejecta sediments can account for infilling of the crater.

Near-rim rock heights and shapes relative to the expected original versus remnant ejecta thickness indicates ~40 cm deflation occurred.

Continued exposure of later arriving, small ejecta rocks in the hollow supports very low estimates of degradation over most hollow history.

Introduction

The *InSight* mission (Interior Exploration using Seismic Investigations, Geodesy, and Heat Transport) to Mars landed November 2018 in western Elysium Planitia at 4.502°N, 135.623°E on a regolith-covered, Early Amazonian basaltic lava plain capped by ~3 m of impact-formed regolith (Banerdt et al. 2020; Golombek, Williams et al., 2020; Golombek, Warner et al., 2020). The lander is within a highly degraded, ~400-700 Myr old, ~27 m-diameter impact crater dubbed “*Homestead hollow*” (Golombek, Warner et al, 2020; Grant et al., 2020; Warner, Grant et al. 2020). The present form of the hollow (Fig. 1) contrasts with its predicted pristine morphology: the original ~0.7 m high rim and ~3-4 m depth has been reduced to a subtle depression only 0.3 m deep. Corresponding estimates of hollow infilling are between 3-4 m (Grant et al., 2020; Warner, Grant, et al., 2020). The surface of the interior of the hollow is characterized by relatively fewer/smaller rock fragments with respect to the margin and near-rim of the exterior (Fig. 2), though there are ~3X more rocks in an area dubbed “*Rocky Field*” on the western interior floor relative to the eastern interior floor (Figs. 1 and 2).

Rocks at *InSight* are basaltic in composition and likely of volcanic lava origin based on: (1) relative proximity to north-south trending wrinkle ridges (Golombek et al., 2018); (2) the presence of degraded lobate flow margins in the region (Golombek et al., 2018); (3) occurrence of platy and ridged surface textures and possible lava inflation plateaus and volcanic vents (Pan et al., 2020); (4) rocks with a fairly uniformly fine-grained aphanitic texture (Golombek, Warner et al., 2020); (6) the absence of any observable sedimentary structures in rocks at the landing site; and (7) evidence that the regional Hesperian transition unit around the lander (Tanaka et al., 2014) experienced an Early Amazonian-aged resurfacing event linked to regionally occurring late volcanism (Warner et al., 2017).

Prior studies concluded that hollow degradation was dominated by eolian and mass wasting processes with lesser impact contributions that stripped and lowered the near-rim and ejecta, resulting in nearly complete infilling of the crater interior and burial of any rocks lining the hollow (Golombek, Warner et al., 2020; Grant et al., 2020; Warner, Grant, et al., 2020). Early degradation of the hollow was relatively more rapid and dominated by deflation of fines from the ejecta, some of which were transported downwind and infilled the crater, and was accompanied by mass-wasting along the crater wall. Early degradation continued until coarser fragments created a surface lag on the ejecta and/or sufficient relief around partially exposed rocks created a boundary layer that precluded further stripping while accumulating eolian fill stabilized the walls of the hollow (Grant et al., 2020; Warner, Grant, et al., 2020). Comparisons made using orbital data covering nearby, similar-sized craters in varying stages of degradation (Sweeney et al., 2018; Warner, Grant, et al., 2020) revealed that *Homestead hollow* assumed something close to its present form within the first 0.05-0.1 Ga after formation (Grant et al., 2020; Warner, Grant, et al., 2020a). At least some rocks visible in the hollow (e.g., *Rocky Field* on the western side; see Golombek, Warner et al, 2020) are likely related to ejecta from subsequent, nearby impacts, and are therefore not associated with hollow formation: their continued partial exposure highlights evidence for very slow modification that occurred over most of the history of the hollow (Grant et al., 2020; Warner, Grant, et al., 2020). The cumulative result of hollow degradation is characterized primarily by an increase in the number and relative relief of rocks along the margin and exterior of the hollow relative to the filled interior (Fig. 2), and there is no significant topographic transition between the two areas (Warner, Grant, et al., 2020). Nevertheless, the relative relief and shapes of rocks in and around the hollow has not been quantified, and thus possible implications for the amount of exterior stripping and accompanying infilling relative to mass wasting or direct infilling related to ejecta from later impacts are not yet been well-defined.

Rock height (vertical measurement of the rock above the adjacent local surface) and three-dimensional shape (various comparisons between the short, intermediate and long axes of a rock) are important parameters used to assess the varying amount and number of geomorphic processes affecting a landscape over time and help identify where erosion dominates over burial and/or help to identify locales where new materials may have been introduced as infilling deposits (Fig. 2).

Rock shape can also be used to help identify the processes and intensity of degradation processes responsible for the characteristics of a rock population, thereby informing (or constraining) which processes have been active and how they may have varied with location over time. A number of studies have examined the two- and three-dimensional shape of rocks (i.e., using either two or three of the principal axes of a rock) on the Earth and Mars. Two-dimensional rock shape characterization can focus on sphericity (Corey, 1949), angularity (Krumbein, 1941) or other characteristics of a rock and is often applied to rocks on Mars where information on all three principal rocks axes is precluded by lack of accurate height information (e.g., Garvin et al., 1981; Yingst et al., 2007, 2008, 2010, 2013; Craddock and Golombek, 2016). Three-dimensional evaluation of rock shapes requires accurate measure of all dimensions and can include various ratios or relations between the long, intermediate, and short axes of a rock (e.g., Zingg, 1935; Sneed and Folk, 1958). These relationships are used to characterize rocks as more rounded (compact or equant), disc-shaped, bladed, or elongate (rod). As general examples, Graham and Midgley (2000) showed that three-dimensional rock form is a discriminator between scree, moraine, and frost-shattered deposits. Three-dimensional shape characteristics for terrestrial basalt rocks in a wide range of geologic and weathering environments, including impact, however, show little variability (e.g., Craddock and Golombek, 2016; Ehlmann et al., 2008; Kumar et al., 2014), likely a reflection of control by cooling fractures on how the rocks break (Craddock and Golombek, 2016). Three-dimensional information related to rock axes at *InSight* is available via processing of stereo images acquired by the lander, enabling direct comparison of rock shapes on Mars to those associated with basalt rocks on the Earth.

Our analysis of variations in the height and shape of basalt rocks around the *InSight* lander can provide additional constraints on geomorphic processes active at the landing site over time to further constrain the responsible processes, their timing, and amount that resulted in hollow degradation. For example, variations in rock height together with information of degradation processes can quantifying differences in relief from

outside to within the hollow that relates to regions of net erosion versus deposition. Moreover, the relief on rock fragments in ejecta around the hollow, where stripping likely predominates, can be equated to the amount of surface lowering that has occurred when coupled with expectations of the pristine thickness and nature of the deposit. We also explore whether there are significant differences in three-dimensional rock shapes at *InSight* relative to the more uniform shapes observed in terrestrial basalt rocks in a range of environments (e.g., Ehlmann et al., 2008; Kumar et al., 2014; Craddock and Golombek, 2016) and examine how differences in shape may relate to their immediate setting and/or formation and modification of the hollow. For example, the observed versus expected form of the basalt rock fragments outside the hollow coupled with rock relief and expectations of the pristine ejecta thickness can help to predict the degree to which rocks remain embedded in the regolith versus being fully exposed on the surface, further informing the amount of stripping that has occurred. We focus on comparison of shape parameters for the basalt rocks at *Homestead hollow* to shape parameters for basalt rocks in the ejecta deposit at the simple-structure Lobar impact crater, in India (Kumar et al., 2014) to minimize any unlikely, minor uncertainties in interpretation related to differences geologic setting. Our approach helps detail where and how much degradation occurred at the *InSight* landing site, and whether processes occurring locally on and within the hollow can account for the current degraded appearance or whether additional sediments from more distant sources are also required. The approach provides a template that can be used to constrain degradation occurring on widespread, broadly similar volcanic surfaces (e.g., Grant et al., 2004, 2020; Tanaka et al., 2014; Warner, Schuyler, et al., 2020) emplaced over latter portions of Mars history.

Measuring Rock Dimensions

The orthogonal dimensions (minimum and maximum horizontal together with height) of rocks around the *InSight* lander were measured from an orthomosaic digital elevation model (DEM) covering much of the nearfield surrounding the lander. Image mosaics of the surface surrounding the landing site were acquired using the arm-mounted Instrument Deployment Camera (IDC, angular resolution of 0.82 mrad/pixel at the center of the image, see Maki et al., 2018). A nearly complete panorama was taken of the landscape around the lander and consists of 283 IDC stereo images (Fig. 2). These images were used to create the orthoimage and DEM of the local environment (Fig. 3). As summarized from Golombek et al. (2021), IDC image resolution varied from 0.12 cm/pixel to 2.8 cm/pixel with increasing range and the DEM has elevation postings every 5 mm. The panorama orthomosaic was bundle adjusted (Abarca et al., 2019), except for the west region, which is separate from the rest of the panorama (Figs. 2 and 3). Error in stereo coordinates is the result of uncertainty in the robotic arm position and stereo processing errors. Nevertheless, pre-launch tests of the surface in front of the lander had a mean horizontal accuracy of 11 mm, a mean absolute vertical accuracy of 6.5 mm, and mean relative vertical accuracy of 5 mm. After landing, 56 images taken in front of the lander on sol 12 and had a spatial accuracy between adjacent stereo frames of 1.9 mm overall with a maximum error between frames of 4 mm. Images further from the lander, including horizon images, were bundle adjusted to those close to the lander. The error within each stereo pair is characterized by the stereo range error (Maki et al., 2018) of the IDC camera, and range error in the DEM increases from <1 cm to ~13 cm at a distance of 10 m from the lander. Spatial uncertainties in the orthomosaic of <4 mm in the workspace to <1 cm at 10 m distance do not have an appreciable effect on derived rock sizes because they are based on relative measurements of rocks over small distance within the orthomosaic and the spatial uncertainties are smaller than that associated with the overall orthomosaic. Golombek et al. (2021) further estimated that the IDC pixel-scale is 0.5 cm at 5 m distance and that 80-95% of the rocks in the DEM down to 0.01 m diameter could be counted out to 10 m. Finally, it is unlikely that a significant number of small rock fragments are undercounted along the hollow margin and exterior as a result of shadowing by larger blocks because of the height of the IDC during imaging (above the lander deck) and the limited range of the measurements. With these points in mind, rock fragments >1 cm were measured within 10 m of the lander that covers a significant portion of the hollow interior, the hollow margin to the west-north and nearest few meters of the hollow exterior to the west-north (Fig. 3).

For the horizontal dimensions of the rock fragments in and around the hollow, we utilized a population of 2,034 rock fragments examined by Golombek et al. (2021) that characterized the rock size-frequency

distribution. As summarized from Golombek et al. (2021), horizontal rock dimensions were made by digitizing polygonal outlines of visible rocks in the orthomosaic in ArcGIS. A convex hull was calculated providing minimum and maximum (non-vertical) axes enclosing a rock. The minimum axis is calculated as the shortest distance between any 2 vertices of the minimum bounding polygon while the maximum axis is calculated as the longest distance between any 2 vertices of the minimum bounding polygon. These measurements are exactly horizontal with no elevation information, yielding the small and large axes for each rock fragment. To measure the height of each fragment, we used the same dataset of 2,034 rocks noted above (Golombek et al. 2021), but removed rocks that were not entirely covered by the 5 mm DEM. The height (Z) of each rock was derived from the 5mm DEM (with 0.5-1 mm vertical precision) using the Add Surface Information plug-in in ArcGIS which calculated the difference between the maximum (Z_MAX) and minimum (Z_MIN) values for each fragment (as mapped by the bounding polygon). Measurements are rounded to the nearest centimeter to maximize confidence in the estimated dimensions. Our final database of rock dimensions includes 2,004 rocks (Fig. 3), distributed in three areas: A) the hollow interior (n=1,850, including *Rocky Field* and more rock-free portions of the interior); B) the hollow margin (n=68) defined as rocks within ~1 m of the zone of increased rock density relative to the hollow interior (Fig. 2); and C) the hollow exterior (n=85) within a few meters beyond the hollow margin to the west-northwest of the lander. Fragment dimensions (minimum horizontal, maximum horizontal, and height) were used to evaluate any systematic changes in rock height or shape within the hollow interior, along the hollow margin, or exterior to the hollow. Our initial assumption is that the rock sizes lining the interior and along the wall (margin) and near-rim should all be generally similar given they are the last materials being excavated during crater formation (average rock size should decrease with increasing distance from the rim). It is likely, however, that increasing thickness of fill from the margin towards the hollow interior results in at least partial burial of many rocks emplaced during the impact-formation of the crater.

Measuring Rock Shape

Rock shapes for fragments in and around the *Homestead hollow* were derived using commonly used calculations (Sneed and Folk, 1958) for maximum projection sphericity (φ), deviation from compactness (D), and form factor (F):

$$\varphi = \sqrt[3]{\frac{S^2}{LI}} \quad (1)$$

$$D = \frac{S}{L} \quad (2)$$

$$F = \frac{L-I}{L-S} \quad (3)$$

Where L , I , and S correspond to the *long*, *intermediate*, and *short* axes of each rock fragment, respectively. Ratios of the length of each axis are then plotted to obtain the form factor using the equations (1)-(3) in the TRI-PLOT excel program published by Graham and Midgley (2000) to constrain the distribution of compact, platy, bladed, and elongate fragments. In addition, the ratios of the rock fragment intermediate to long axis versus fragment short to intermediate axis was plotted separately (after Zingg, 1935) to characterize whether fragments are more equant, discoidal, bladed, or rod-shaped relative to expectations from studies of terrestrial basalt rocks (e.g., Ehlmann et al., 2008; Kumar et al., 2014; Craddock and Golombek, 2016).

Results

Rock heights on the exterior, margin, and interior of the hollow (Fig. 3) are often the shortest measured axis (height is the short axis 78% of exterior rocks, 91% of margin rocks, and 97% of interior rocks) (Table 1, see also Grant et al. (2021) data repository for additional details). For the exterior of the hollow, the 10 tallest rocks stand between 23-30 cm in exposed relief (five largest rocks are >28 cm in height), and 22% of the rocks are >10 cm tall. The 10 tallest rocks along the hollow margin stand between 4-33 cm in exposed relief (five largest rocks are 25-34 cm in height), with 10% of the rocks > 10 cm tall. In the hollow interior, the 10 tallest rocks stand between 14-26 cm in exposed relief, but less than 1% of the rocks are > 10 cm tall (Table 1). The decrease in rock height from the exterior to the interior of the hollow is also apparent in the overall average height of rocks within each zone, with rocks outside the hollow, around the hollow margin,

and inside the hollow measuring 6 cm, 4 cm, and 1 cm tall, respectively (Table 1, Fig. 4). The standard error associated with the height in each zone indicates that the differences are significant (Fig. 4), especially between the exterior and the interior of the hollow. To evaluate whether the difference in the height of rocks outside versus within the hollow is related to larger versus smaller rocks within the hollow, height values were normalized by dividing the rock height by the average of the width and length. Resultant values for the exterior rocks are 0.42 (0.65 standard deviation) versus 0.27 (0.34 standard deviation) and 0.25 (0.42 standard deviation) for the margin and interior rocks, respectively. These values are consistent with a wide range in rock sizes in all three areas, but that are generally higher and more exposed around the exterior of the hollow.

With the above in mind, study of rock shape focused on rock fragments on the exterior and margin of the hollow (see also Grant et al. (2021) data repository for additional details) because they are more exposed, consistent with predictions (Golombek, Warner, et al., 2020; Grant et al., 2020; Warner, Grant, et al., 2020). For exterior fragments, the maximum projection sphericity (equation 1) ranges from 0.11 to 0.87 with a mean of 0.35 (0.21 standard deviation) and from 0.10 to 0.81 with a mean of 0.33 (0.15 standard deviation) for the margin (Table 1). The deviation from compactness (equation 2) is 0.02 to 0.74 with a mean of 0.18 (0.18 standard deviation) for the exterior and from 0.02 to 0.73 with a mean of 0.16 (0.13 standard deviation) for the margin (Table 1). The form factor (equation 3) for the exterior ranges from 0.18 to 0.97 with a mean of 0.57 (0.18 standard deviation) for the exterior and from 0.05 to 0.90 with a mean of 0.52 (0.17 standard deviation) for the margin (Table 1). By comparison, basalt rock fragments in the ejecta deposit at Lonar crater have a maximum projection sphericity 0.11 to 1.0 with a mean of 0.72, the deviation from compactness is 0.18 to 1.0 with a mean of 0.53, and the form factor ranges from 0 to 1 with a mean of 0.56 (Table 1). As such, the most similar shape parameter between the rock fragments at *InSight* and in the ejecta at Lonar crater is the form factor. When plotted (Sneed and Folk, 1958; Zingg, 1935) and compared to the shape of basaltic fragments in ejecta at Lonar crater (Kumar et al., 2014) large differences can be seen (Figs. 5 and 6): the rock fragments in all three zones in and around the hollow at *InSight* appear significantly more platy, bladed, and elongate in the triangular form factor plot (Fig. 5) and the bulk of fragments inside the hollow are discoidal and bladed and rocks along the hollow margin and exterior are more bladed in the axes ratio plot (Fig. 6). By contrast, the rock fragments at Lonar are mostly compact, compact platy, compact bladed, compact elongated, platy, bladed, and elongate in the triangular form factor plot (Fig. 5), whereas ejecta fragments at Lonar are mostly equant with lesser, but significant disc- and blade-shaped fragments in the axes ratio plot (Fig. 6). Although Lonar is a relatively fresh impact crater where rocks have been subjected to more rapidly weathering versus the very degraded appearance of *Homestead hollow*, evaluation of basalt rock shapes from diverse geologic and weathering environments on Earth indicates there should be little effect on expected rocks shapes (Craddock and Golombek, 2016).

Discussion

The greater rock height outside the hollow is confirmed after normalizing for possible variations in overall rock size that indicates differences are not solely the result of larger versus smaller rocks around and within the hollow (Fig. 4). This observation coupled with an increasing percentage of rocks where height corresponds to the measured short axis from outside to around to within the hollow supports the greater exposure of rocks on the near rim relative to the interior and is consistent with inferred degradation of the hollow dominated by stripping fines from the exposed ejecta deposit accompanied by downwind deposition and infilling of the hollow (Golombek, Warner et al., 2020; Grant et al., 2020; Warner, Grant, et al., 2020). Reasonable expectations of relative rocks sizes around and within the pristine crater, however, suggest that the difference in rock height between the exterior and interior of the hollow is not a simple reflection of the difference between the total of exterior stripping versus interior infilling that has occurred.

Examination of the ejecta remnants around *Homestead hollow* and other fresh, nearby small craters reveals only a few meter-scale rocks (Golombek, Williams et al., 2020; Warner et al., 2017) and implies those lining the original floor and walls of the hollow are of a similar scale and are of a lesser size than the depth of fill. This contention is supported by the paucity of rocks observed in HiRISE images of craters <30-40 m

in the vicinity of the landing site (Warner et al., 2017) and the expectation that the original 3-4 m depth of the hollow largely limited impact excavation to the pre-existing impact regolith (Banerdt et al., 2020; Golombek, Williams et al., 2020; Golombek, Warner et al., 2020) rather than excavating larger rocks from more competent material below that could yield larger rocks (that result in Rocky Ejecta Craters or RECs, see Warner, Grant, et al., 2020). In addition, the local regolith has locally experienced approximately three impact events that would be responsible for breaking any large blocks into smaller fragments (Charalambous et al., 2020; Golombek et al., 2018, 2021). However, even if the hollow-forming impact occurred into bedrock, the maximum expected fragment size of 0.9-2.8 m (based on the relation between crater size and largest associated rock described in Moore (1971) makes it very likely that rocks lining the original hollow floor are buried beneath the fill (Grant et al., 2020). Hence, the difference in rock height between the exterior and interior of the hollow is only a partial reflection of the deflation versus infilling that has occurred. More likely, the generally smaller size and distribution of exposed interior rocks (e.g., forming *Rocky Field*) is consistent with later arriving ejecta fragments from nearby impacts as described in Grant et al. (2020) that have since been partially buried.

Nevertheless, consideration of the rock height/exposure on the near-rim relative to expected characteristics of the pristine ejecta can be used to understand the amount of deflation that has occurred there. To start, the approximate pristine ejecta thickness around the hollow can be estimated using:

$$E_t = 0.14R_t^{0.74}(r/R_t)^{-3.0}(4)$$

Where the ejecta deposit (E_t , measured in meters) can be related to the transient crater radius R_t (where the transient crater diameter D_t is $0.84D$ (D is the final diameter)) and radial distance r from the crater rim, where $r > R_t$ (McGetchin et al., 1973). Predicted ejecta thickness around the pristine *Homestead hollow* ranges from ~50 cm at the rim to around 30 cm three meters outside the rim, 20 cm five meters beyond the rim, 10 cm at 1 radius, and only a couple of cm at 1 D range.

Based on analogy with ejecta deposits around Meteor Crater, AZ, (Grant and Schultz, 1993) and Lonar crater (Kumar et al., 2014), the pristine ejecta deposit around *Homestead hollow* likely graded from more clast rich, perhaps clast supported, to matrix rich, perhaps matrix-supported deposit with increasing radial distance from the rim. Although thinner, ejecta further from the rim was likely characterized by fewer large fragments and more abundant fines, and may have supplied relatively more sediment (i.e., per unit volume) for transport due to a lesser abundance of lag or surface armoring fragments. Moreover, the multiple impact gardening of the regolith into which *Homestead hollow* formed would have produced abundant sand-sized material at the expense of fewer larger rocks in accordance with expectations from fragmentation during three impact events (Golombek, Charalambous et al., 2020; Golombek et al., 2018, Golombek et al., 2021). Finally, the numerous rocks that are exposed around the margin and exterior of *Homestead hollow* implies the hollow-forming impact did not occur into pre-existing fines filling an older crater, in which case even more fines and fewer clasts would be expected (Grant et al., 2020). In any of these situations, variable numbers of relatively large (10s of cm up to ~1 m) fragments would likely be present, but more common/numerous in the vicinity of the rim-crest.

Hence, the pristine ejecta deposit around the hollow was likely characterized by a wide range of fragment sizes, but with a paucity of large fragments standing in significant relief. The pristine surface would have been in disequilibrium with regional geomorphic thresholds (Grant et al., 2020; Warner, Grant, et al., 2020) and susceptible to deflation that would have continued until fragments too large to be transported accumulated as an armoring lag and/or increasing rock relief created boundary layer that precluded further eolian transport (Grant et al., 2020). With these points in mind, differing amounts of amount of eolian deflation from the ejecta around the hollow can be approximated and compared to the volume associated with fill inside the hollow.

The volume of fill within the 27 m-diameter hollow can be constrained to first order using an original depth of ~3-4 m that is now 0.3 m post-infilling (Warner, Grant, et al., 2020) and yields a total fill volume of ~500-700 m³. If on order of 60% of the infill is due to diffusional infilling from around the hollow and 40% is due to

eolian infilling (based on evaluation of ~ 100 m-diameter craters in the region, Sweeney et al., 2018) then the eolian contribution to infilling is ~ 200 - 280 m³. The small size and limited pristine depth of *Homestead hollow* suggests steep slopes facilitating diffusional infilling were of limited extent and would have been stabilized by increasing accumulation of eolian infill. Hence, the actual eolian component to infilling may have been somewhat greater than 40%.

It is unlikely that the 6 cm greater average relief of fragments on the near-rim of the hollow reflects a uniform amount of ejecta stripping from the entire deposit given the greater exposed relief on many of the near-rim rocks (as compared to the likely appearance of the pristine deposit) and the limited thickness of ejecta beyond about 1R from the rim. (Golombek, Warner et al, 2020; Grant et al., 2020; Warner, Grant, et al., 2020). Despite that, an average of 6 cm deflation to a distance of 1D from the rim would supply ~ 300 m³ of sediment, close to what is required if all the all of the fill was eolian. Prevailing, reversing northwest-southeast winds (Spiga et al., 2018), however, would cause a significant fraction of sediment to be transported downrange and bypass the hollow. If half of the deflated sediment was blown back into the hollow, the volume contributing to infilling could be ~ 150 m³ and somewhat less than the lower end estimate of a 40% eolian contribution to the total fill volume. A more realistic estimate of the eolian erosion from the ejecta might be obtained from the relief on exposed near-rim rocks, given most were likely buried or expressed limited relief in the pristine deposit, coupled with use of a decreasing amount of deflation with increasing range that better reflects the decreasing thickness of ejecta with increasing distance from the rim. The maximum relief of rocks around the hollow is ~ 0.3 m as measured in the DEM and there are a few instances of rock relief as large as 0.4 m (First Rock, ~ 20 m distance) and 0.5 m (Hanging Rock, ~ 21 m distance) beyond the limit of the DEM (Golombek, Williams et al, 2020; 2021). Based on those rock heights and estimates of pristine ejecta thickness that decrease outside the rim, deflation of 0.4 m to a range of 3 m beyond the rim, 0.25 m between 3-5 m beyond the rim, 0.13 m 5-15 m beyond the rim, and 0.03 m from 15-27 m beyond the rim yields a sediment volume of ~ 440 m³. While this exceeds the volume of the expected eolian contribution to hollow infilling, it is a reasonable match if $\sim 50\%$ is blown back into the crater by the prevailing winds and the remaining deflated sediments bypassed the hollow. If the volume of fill in the hollow is on the lower end of estimates and/or a slightly larger percentage of deflated sediments are blown back into the crater, then eolian contributions could approach 50% or slightly more, but likely would not comprise an overwhelming fraction of the infilling sediments.

Rock shapes at *Homestead hollow* provide an independent check on whether our deflation estimates are realistic. In contrast to the expectation of mostly compact, compact platy, compact bladed, compact elongated, platy, bladed, and elongate rocks (Fig. 5) or mostly equant ($\sim 1/3$ of the total) with lesser, disc- and blade-shaped fragments (Fig. 6) at *InSight* based on comparison to rocks at Lonar crater (and elsewhere, Ehlmann et al., 2008; Kumar et al., 2014; Craddock and Golombek, 2016) there is a preponderance of platy, bladed, and elongate rocks. Further, at *Homestead hollow*, the average maximum projection sphericity (equation 1) of 0.35 and average deviation from compactness (equation 2) of just under 0.2 are well below the average of 0.72 and 0.53, respectively, of fragments measured at Lonar crater. However, the form factor (equation 3) for fragments at *InSight* averages 0.5-0.6 and is comparable to the average of 0.56 observed at Lonar and may hold a clue to understanding the cause of other differences.

Possible reasons for apparent differences in rock shape parameters at *InSight* include: A) error in measurements made in the direction viewed from the lander if the fragment profile precludes accurate measure of dimensions; and/or B) the partially buried nature of the *InSight* fragments (especially inside the hollow) leads to underestimate of the axis associated with rock height. The former can be ruled out because there is no systematic change in the shape parameters with increasing distance from the lander when viewed more obliquely.

For the second possibility, the partially embedded appearance of many of the near-rim rocks, and more buried appearance of rocks within the hollow, suggests that the actual rock heights are being underestimated. The predominance of rock height as the smallest fragment axis, provides support for this statement. For example, height acts as the short axis for a large majority (78%) of the fragments on the near-rim and suggests that

underestimation of rock height is skewing the shape analyses. Equations (1) and (2) emphasize the smallest rock axis in the numerator that can lead to lesser estimated values of maximum projection sphericity and deviation from compactness. By contrast, the form factor includes the smallest axis of each fragment as a difference in the denominator and could have a lesser impact on the calculated values that appear to better match what is seen in the *InSight* versus terrestrial rocks.

In order to consider the effects of underestimating rock height on derived rock shapes, we recalculated shape parameters and plots after addition of relief to rocks on the near-rim to account for their partially embedded appearance. We focused on fragments around the exterior of the hollow because they are the best exposed (based on greater rock relief and somewhat lesser percentage of measured height as the short fragment axis) and made comparisons to the maximum estimated thickness of the original ejecta deposit.

The estimated 30-50 cm original thickness of pristine ejecta within a few meters of the hollow rim (covered by the DEM) coupled with the ~30 cm relief on some partially embedded fragments in the same zone makes it reasonable that an average ~10 cm ejecta (plus/minus) buries the base of many fragments. Accordingly, 10 cm was added to the height of each rock on the exterior of the hollow as an estimate for the rock fraction that remains embedded/buried and resultant revised heights were used in recalculation of shape parameters. The revised average values for maximum projection sphericity are 0.65 (0.09 standard deviation, range between 0.29 and 0.85), compactness is 0.45 (0.11 standard deviation, range between 0.11 and 0.68), and form factor is 0.49 (0.26 standard deviation, range 0.01 and 0.95), all much closer to the corresponding values of 0.72, 0.53, and 0.56 for ejecta fragments at Lomar crater, respectively. The resultant updated data cloud for exterior rocks including the revised heights are shown in the TRI-PLOT (Sneed and Folk, 1958) and mostly superposes the data cloud for rocks in the ejecta at Lomar crater. Results suggest that continued ~10 cm embedding of the near-rim exterior rocks can account for most of the observed differences in rock shape between *Homestead hollow* and what is expected from basalt rocks at Lomar crater (Kumar et al., 2014) and in other terrestrial locations (e.g., Ehlmann et al., 2008; Craddock and Golombek, 2016). Hence, ~30 cm or slightly more deflation from the near-rim (decreasing outwards) is supported by greater near-rim rock heights, deflation estimated from the near-rim based on comparison of rock height and original ejecta thickness, and consistency between revised rock relief, estimated original ejecta thickness, and expected rocks shapes.

Interior rocks provide additional clues to the degradation history of the hollow. Rocks inside the hollow average ~1 cm in height and more than >99% are less than 10 cm tall and it is likely that most or all are distal ejecta delivered during nearby impacts (Grant et al., 2020). Those associated with *Rocky Field* were likely emplaced within the first 0.1 Ga of hollow history (Sweeney et al., 2018; Grant et al. 2020; Warner, Grant, et al., 2020). Although the actual size of the interior fragments is uncertain due to their partial burial, the ratio of their height to average width and comparison to average size of more exposed rocks on the rim coupled with likely emplacement as distal ejecta (Grant et al. 2020) suggests most are small and likely less than 10 cm tall. Warner, Grant, et al. (2020) and Grant et al. (2020) estimated initially high degradation rates during the first ~0.1 Ga after hollow formation quickly slowed as surrounding ejecta became armored by a coarse lag and/or increasing surface relief due to around larger rocks created a boundary layer that precluded eolian transport. Degradation rates following this early period were estimated to be 10^{-4} m/Myr for most of the 0.4-0.7 Ga history of the hollow (Sweeney et al., 2018; Warner, Grant, et al. 2020) equating to ~3-6 cm of infilling since emplacement of the fragments forming *Rocky Field*. The likely small size, but continued, limited exposure of the fragments in *Rocky Field* and other interior rocks is consistent with these estimates of very slow degradation over the bulk of hollow history.

Our results provide a new means for constraining hollow degradation that is consistent with prior predictions of modification history. The exposed rock relief and revised rock shapes on the near-rim support deflation of up to 40 cm at the near-rim, decreasing with range, and is a good match with expected eolian contributions of 40% or slightly more to hollow infilling: the remainder of infilling is likely the result of diffusional processes (Sweeney et al. 2018; Warner, Grant, et al., 2020) with only minimal additional infilling contributions associated with eolian transport from ejecta around later forming craters. Instead, the inventory of deflated

ejecta sediment bypassing the hollow likely contributed to eolian bedforms in the vicinity of the landing site (e.g., Golombek, Warner, et al., 2020).

Further, limited hollow infilling via deflation off ejecta around later impacts is consistent with early, more rapid infilling followed by very slow degradation over the bulk of hollow history. Continued exposure of *Rocky Field* and other interior rocks supports this model. Small rocks forming *Rocky Field* were likely emplaced during the first ~ 0.1 Ga after the hollow formed (Grant et al., 2020; Warner et al., 2020) on a surface close to what is observed in the hollow today. And their continued exposure is inconsistent with more significant infilling associated with eolian transport from ejecta around later occurring impacts.

Summary

The rocks heights and shapes around and within *Homestead hollow* provide independent evidence regarding degradation over time that are generally consistent with processes inferred from prior studies (Golombek, Warner, et al. 2020; Grant et al., 2020; Warner, Grant, et al., 2020). Decreasing average rock height, decreasing largest (exposed) fragment size, and increasing percentage of fragments where height is the short axis characterize rocks from outside to within the hollow. These observations coupled with evaluation of likely pristine ejecta thickness and properties support net stripping of the ejecta of up to ~ 40 cm in the near-rim and eolian contribution of 40% or slightly more to the inventory of sediments filling of the hollow. Moreover, differences between observed versus expected rock shapes on the exterior of the hollow are found to relate mostly to underestimating rock height as a result of continued ~ 10 cm embedding of near-rim fragments in the remnant ejecta deposit. Recalculation of rock shapes to accommodate an average additional height of ~ 10 cm leads to a close match to expected terrestrial basalt rock shapes Earth (e.g., Ehlmann et al., 2008; Kumar et al., 2014; Craddock and Golombek, 2016) and further constrains near-rim deflation to around ~ 30 cm or slightly more (with an additional ~ 10 cm remaining). Continued exposure of rocks within the hollow (e.g., *Rocky Field*) support estimates of only 10^{-4} m/Myr degradation for most of the 0.4-0.7 Ga history of the hollow (Sweeney et al., 2018; Warner, Grant, et al. 2020). Results suggest that a significant fraction of sediments deflated from the ejecta bypass the hollow via prevailing winds and are likely trapped by local topography, with some contributing to numerous nearby bedforms rather than appreciable infilling of downwind impact structures.

The estimated amount of degradation inferred from rock relief and shape around and within *Homestead hollow* helps to quantify, and is consistent with, both the current and predicted initial appearance of the crater as well as the estimated amount of modification and geomorphic processes it has experienced since formation (Golombek, Warner, et al., 2020; Grant et al., 2020; Warner, Grant, et al., 2020). Because volcanic surfaces of intermediate to young age are widespread on Mars (Tanaka et al., 2014), evaluation of rock heights and shape around small impact craters can be an important tool for understanding local degradation history

Acknowledgements, Samples, Data

We thank the Jet Propulsion Laboratory, Lockheed Martin Space Systems, CNES, and other partner institutions that built and operate the *InSight* lander. A portion of the work was supported by the InSight Project at the Jet Propulsion Laboratory, California Institute of Technology, and under grants 80NSSC18K1625 to J. Grant (includes S. Wilson and C. Weitz) and 80NSSC18K1624 to N. Warner from the National Aeronautics and Space Administration. All data used in the paper is freely accessible at the link provided below in the Data Availability Statement that follows. This is InSight Contribution Number 229.

Data Availability Statement

All data used in analyses of rocks at the InSight lander and described in the paper are included in two Microsoft 365 Excel files (and associated readme explanation Word file) and ArcGIS shape files (and associated readme explanation Word file, and orthophoto and DEM) that can be freely accessed and downloaded for viewing at Smithsonian.figshare: <https://doi.org/10.25573/data.15121554>.

References

- Abarca, H., Deen, R., Hollins, G., Zamani, P., Maki, J., Tinio, A., et al. (2019). Image and data processing for InSight lander operations and science. *Space Science Reviews* , 215(2), 22. <https://doi.org/10.1007/s11214-019-0587-9>
- Banerdt, W. B., Smrekar, S. E., Banfield, D., Giardini, D., Golombek, M., Johnson, C. L., et al. (2020). Early results from the InSight mission: Mission overview and global seismic activity. *Nature Geosciences* , 13, 183-189. <https://doi.org/10.1038/s41561-020-0544-y>.
- Charalambous, C. (2014). On the evolution of particle fragmentation with applications to planetary surfaces. PhD Thesis, Imperial College London.
- Craddock, R. A., & Golombek, M. P. (2016). Characteristics of terrestrial basaltic rock populations: Implications for Mars lander and rover science and safety. *Icarus* , 274, 50-72. <https://doi.org/10.1016/j.icarus.2016.02.042>.
- Ehlmann, B. L., Viles, H. A., & Bourke, M. C. (2008). Quantitative morphologic analysis of boulder shape and surface texture to infer environmental history: A case study of rock breakdown at the Ephrata Fan, Channeled Scabland, Washington. *Journal of Geophysical Research* , 113, F02012. <https://doi.org/10.1029/2007JF000872>.
- Garvin, J.B., Mougini-Mark, P.J., & Head, J.W. (1981). Characterization of rock populations on planetary surfaces: Techniques and a preliminary analysis of Mars and Venus. *Moon Planets* , 24, 355–387.
- Golombek, M. P., Grant, J. A., Crumpler, L. S., Greeley, R., Arvidson, R. E., Bell, J. F., III, et al. (2006). Erosion rates at the Mars Exploration Rover landing sites and long-term climate change on Mars. *Journal of Geophysical Research* , 111. <https://doi.org/10.1029/2006JE002754>.
- Golombek, M., Kipp, D., Warner, N., Daubar, I. J., Ferguson, R., Kirk, R. L., et al. (2017). Selection of the InSight landing site. *Space Science Reviews* , 211(1-4), 5–95. <https://doi.org/10.1007/s11214-016-0321-9>.
- Golombek, M. P., Grott, M., Kargl, G., Andrade, J., Marshall, J., Warner, N., et al. (2018). Geology and physical properties investigations by the InSight lander. *Space Science Reviews* , 214, 84. <https://doi.org/10.1007/s11214-018-0512-7>.
- Golombek, M. P., Charalambous, C., Pike, W. T., & Sullivan, R. (2018). The origin of sand on Mars (expanded abstract). *49th Lunar and Planetary Science* , Abstract #2319, Lunar and Planetary Institute, Houston.
- Golombek, M., Williams, N., Warner, N. H., Parker, T., Williams, M. G., Daubar, I., et al. (2020). Location and setting of the Mars *InSight* lander, instruments, and landing site. *Earth and Space Science* , 7, e2020EA001248. <https://doi.org/10.1029/2020EA001248>.
- Golombek, M. P., Warner, N. H., Grant, J. A., Hauber, E., Ansan, V., Weitz, C. M., et al. (2020). Geology of the InSight landing site on Mars: Nature Communications, 11. <https://doi.org/10.1038/s41467-020-14679-1>.
- Golombek, M., Charalambous, C., Pike, W. T., & Sullivan, R. (2020). The origin of sand and dust on Mars: Evidence from the InSight landing site (expanded abstract). *51st Lunar and Planetary Science* , Abstract #2744, Lunar and Planetary Institute, Houston.
- Golombek, M. P., Trussell, A., Williams, N., Charalambous, C., Abarca, H., Warner, N. H., et al. (2021). Rock Size-frequency distribution of the InSight landing site, Mars. *Earth and Space Science* . (in review).
- Graham, D. J., & Midgley, N. G. (2000). Graphical representation of particle shape using triangular diagrams: An Excel spreadsheet method. *Earth Surface Processes and Landforms* , 25(13), 1473 – 1477. [https://doi.org/10.1002/1096-9837\(200012\)25:133.0.CO;2-C](https://doi.org/10.1002/1096-9837(200012)25:133.0.CO;2-C).
- Grant, J. A., & Schultz, P. H. (1993). Erosion of Ejecta at Meteor Crater, Arizona. *Journal of Geophysical Research* , 98, 15,033-15,047.

- Grant, J. A., Arvidson, R. E., Bell, J. F., III, Cabrol, N. A., Carr, M. H., Christensen, P. R., et al. (2004). Surficial deposits at Gusev Crater along Spirit rover traverses. *Science*, 305, 807-810. <https://doi.org/10.1126/science.1099849>.
- Grant, J. A., Warner, N. H., Weitz, C. M., Golombek, M. P., Wilson, S. A., Baker, M., et al. (2020). Degradation of Homestead hollow at the InSight landing site based on the distribution and properties of local deposits. *Journal of Geophysical Research*, 125. <https://doi.org/10.1029/2019JE006350>.
- Grant, J. A., Wilson, S. A., Golombek, M. P., Trussell, A., Warner, N. H., Williams, N., et al. (2021). Data repository for rock dimension data and related plots for fragments around the *InSight* lander, Mars. Smithsonian figshare: see <https://doi.org/10.25573/data.15121554>.
- Senthil Kumar, P., Prasanna Lakshmi, K. J., Krishna, N., Menon, R., Sruthi, U., Keerthi, V. (2014). Impact fragmentation of Lonar Crater, India: Implications for impact cratering processes in basalt. *Journal of Geophysical Research*, 119, 2029–2059. <https://doi.org/10.1002/2013JE004543>.
- Maki, J., Golombek, M. P., Deen, R., Abarca, H., Sorice, C., Goodsall, T., et al. (2018). The color cameras on the InSight lander. *Space Science Reviews*, 214, 105. <https://doi.org/10.1007/s11214-018-0536-z>.
- McGetchin, T. R., Settle, M., & Head J. W. (1973). Radial thickness variation in impact crater ejecta: Implications for lunar basin deposits. *Earth and Planetary Science Letters*, 20, 226-236.
- Melosh, H. J. (1989). *Impact Cratering*, 245 pp., Oxford University Press, New York.
- Moore, H. J. (1971). Large blocks around lunar craters, in *Analysis of Apollo 10 Photography and Visual Observations*. *NASA Special Publication*, SP-232, 26–27.
- Pan, L., Quantin-Nataf, Q., Tauzin, B., Michaut, C., Golombek, M. P., Lognonne, P., et al., et al. (2020). Crust stratigraphy and heterogeneities of the first kilometers at the dichotomy boundary in western Elysium Planitia and implications for InSight lander. *Icarus*, 338. <https://doi.org/10.1016/j.icarus.2019.113511>
- Sneed, E. D., & Folk, R. L. (1958). Pebbles in the lower Colorado River, Texas: A study in particle morphogenesis. *Journal of Geology*, 66(2), 114–150.
- Spiga, A., Banfield, D., Teanby, N. A., Forget, F., Lucas, A., Kenda, B., et al. (2018). Atmospheric science with *InSight*. *Space Science Reviews*, 214, 109. <https://doi.org/10.1007/s11214-018-0543-0>.
- Sweeney, J., Warner, N. H., Ganti, V., Golombek, M. P., Lamb, M. P., Ferguson, R., & Kirk, R. (2018). Degradation of 100-m-scale rocky ejecta craters at the InSight landing site on Mars and implications for surface processes and erosion rates in the Hesperian and Amazonian. *Journal of Geophysical Research*, 123, 2732. <https://doi.org/10.1029/2018JE005618>.
- Tanaka, K., Skinner, J. A. Jr., Dohm, J. M., Irwin, R. P. III, Kolb, E. J., Fortezzo, C. M., et al., et al. (2014). *Geologic map of Mars*, United States Geological Survey Science Investigations. Mappemonde, 3292.
- Warner, N. H., Golombek, M. P., Sweeney, J., Ferguson, R., Kirk, R., & Schwartz, C., (2017). Near surface stratigraphy and regolith production in southwestern Elysium Planitia, Mars: Implications for Hesperian-Amazonian terrains and the *InSight* lander mission. *Space Science Reviews*, 211, 147. <https://doi.org/10.1007/s11214-017-0352-x>.
- Warner, N. H., Grant, J. A., Wilson, S. A., Golombek, M. P., DeMott, A., Charalambous, C., et al. (2020). An impact crater origin for the InSight landing site at Homestead Hollow: Implications for near surface stratigraphy, surface processes, and erosion rates. *Journal of Geophysical Research*, 125. <https://doi.org/10.1029/2019JE006333>.
- Warner, N. H., Schuyler, A. J., Rogers, A. D., Golombek, M. P., Grant, J. A., Wilson, S. A. (2020). Crater morphometry on the mafic floor unit at Jezero crater, Mars: Comparisons to a known basaltic lava plain at the InSight landing site. *Geophysical Research Letters*, 47. <https://doi.org/10.1029/2020GL089607>.

Williams, N., Golombek, M. P., Warner, N. H., Daubar, I. J., Hausmann, R. B, Hauber, E., et al. (2019). Surface alteration from landing InSight on Mars and its implications for shallow regolith structure. *50th Lunar and Planetary Science* , Abstract #2781. *Lunar and Planetary Institute* , Houston.

Yingst, R. A., Haldemann, A. F. C., Biedermann, K. L., & Monhead, A. M. (2007). Quantitative morphology of rocks at the Mars Pathfinder landing site. *Journal of Geophysical Research* , 112, E06002. <https://doi.org/10.1029/2005JE002582>.

Yingst, R. A., Crumpler, L., Farrand, W. H., Li, R., Cabrol, N. A., & Neakrase, L. D. (2008). Morphology and texture of particles along the Spirit rover traverse from sol 450 to sol 745. *Journal of Geophysical Research* , 113, E12S41. <https://doi.org/10.1029/2008JE003179>.

Yingst, R. A., Crumpler, L., Farrand, W. H., & de Souza P. (2010). Constraints on the geologic history of “Home Plate” materials provided by clast morphology and texture. *Journal of Geophysical Research* , 115, E00F13. <https://doi.org/10.1029/2010JE003668>.

Yingst, R. A., Kah, L. C., Palucis, M., Williams, R. M. E., Garvin, J., Bridges, J. C., et al. (2013). Characteristics of pebble- and cobble-sized clasts along the Curiosity rover traverse from Bradbury Landing to Rocknest. *Journal of Geophysical Research* , 118, 2361–2380. <https://doi.org/10.1002/2013JE004435>.

Zingg, T. (1935). Beitrage Zur schotteranalyse, *Schweizerische Mineralogische und Petrographische Mitteilungen* , 15, 39–14.

Table 1 and Figures/Captions

Table 1. Summary of Rock Height and Shape Parameters For Basalt Rocks at *InSight*

Location	Average Rock Height	10 Tallest Rocks	Height Short Axis %	Max Proj. Spher. (Ave./Range)	Dev. Comp. (Ave/Range)	Form Factor (Ave/Range)
Exterior	6 cm	23-30 cm	78%	0.35/0.11-0.87	0.18/0.02-0.74	0.57/0.18-0.97
Margin	4 cm	4-33 cm	91%	0.33/0.10-0.81	0.16/0.02-0.73	0.52/0.05-0.90
Interior	1 cm	14-26 cm	97%	n/a	n/a	n/a
Lunar Ejecta	n/a	n/a	n/a	0.72/0.11-1.0	0.53/0.18-1.0	0.56/0.0-1.0
Exterior >10 cm	n/a	n/a	n/a	0.65/0.29-0.85	0.45/0.11-0.68	0.49/0.01-0.95

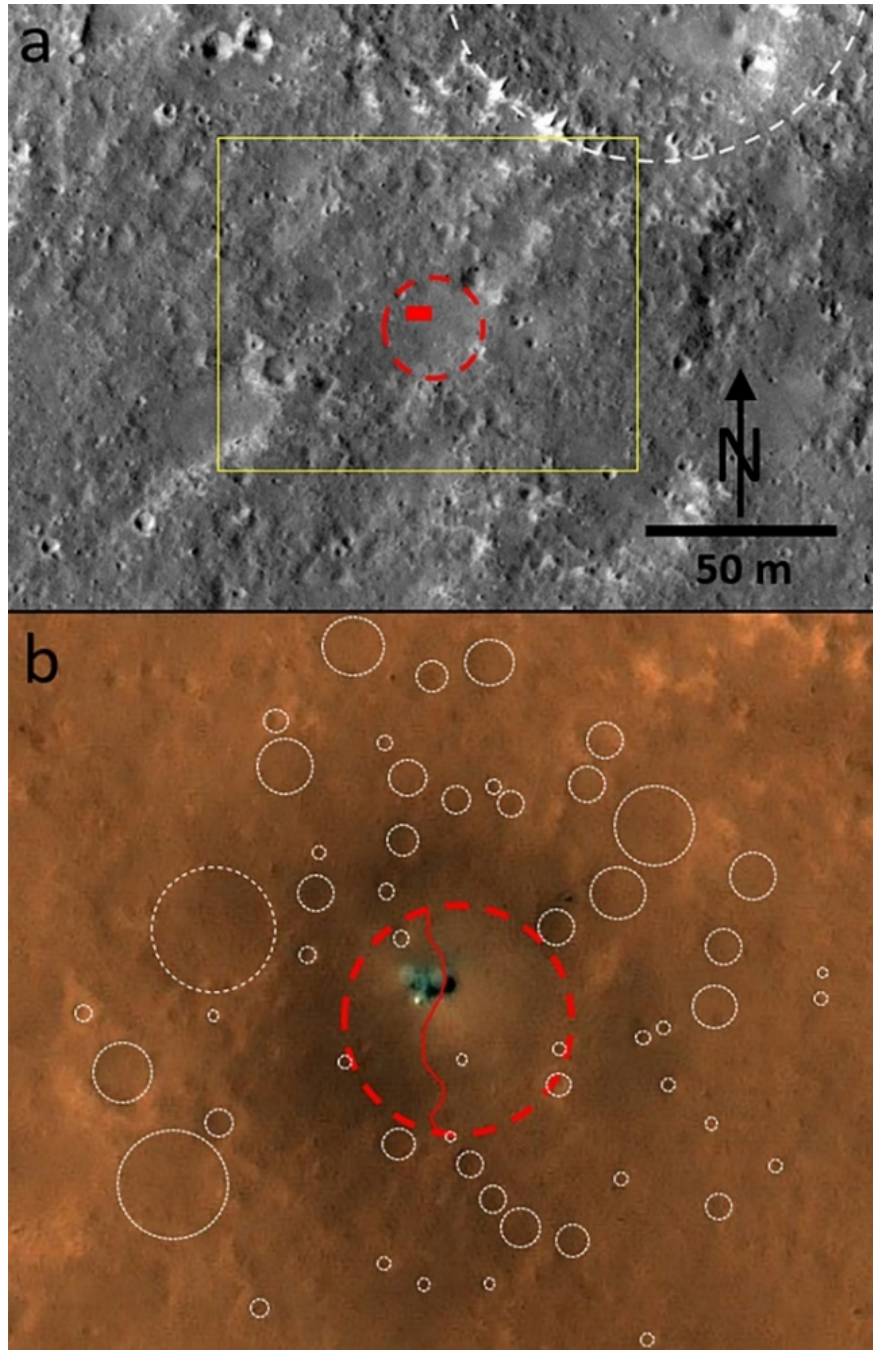


Figure 1. (a) The *InSight* lander (red box) in the 27 m-diameter *Homestead hollow* degraded impact crater (red dashed circle) in western Elysium Planitia, Mars (4.502°N, 135.623°E). The lander is 6 m measured across the solar panels, is in the northwestern quadrant of the hollow, and the lander workspace is to the south. Yellow box shows location of (b). Subframe of HiRISE color ESP_036761_1845 (0.25 m/pixel). (b) Color view of *InSight* lander in *Homestead hollow* (red dashed circle) and other hollows (white dotted circles) in the immediate vicinity. Red line cutting across the hollow is the boundary between occurrence of relatively few rocks to the east versus $\sim 3X$ more rocks in the region to the west dubbed “*Rocky Field*” (see Figure 2). Landing rockets removed dust from the immediate surface and caused the bright zone and surrounding

dark halo around the lander (Williams et al., 2020). Subframe of HiRISE color image ESP_061684_1845 (0.25 m/pixel). Modified from Fig. 1 in Grant et al. (2020).

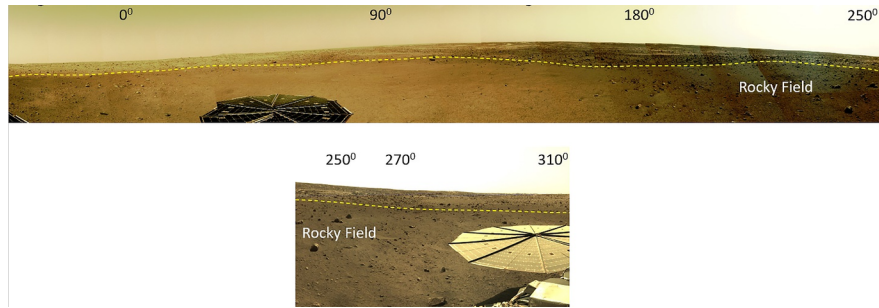


Figure 2. Mosaic covering approximately 290 degrees around the north, east and south side of lander in *Homestead hollow* (top) and mosaic covering approximately 70 degrees around the west side of the lander (bottom). Near- and mid-field coverage in the mosaics matches that shown in the orthomosaic/DEM in Figure 3 and enabled measurement of rocks within 10 m of the lander across a broad swath of the hollow interior, within ~ 1 meter of the margin (yellow dashed line) to the west to the north side of the hollow, and on the west/north near-rim within a few meters outside the hollow rim. For scale, the lander solar panels in both mosaics are 2.15 m in diameter. Rocky Field denotes the $\sim 3X$ higher density of rocks on the west-northwest part of the hollow interior. Numbers refer to azimuth where 0° is true north. Mosaic D_LRGB_0014_RAS030100CYL_R_SCIPANQM1 (a) and IDC Mosaic D_LRGB_0119_RAD030100CYL_R_-AUTOGENM3 (b). Small black areas around mosaic margins are gores in the image data.

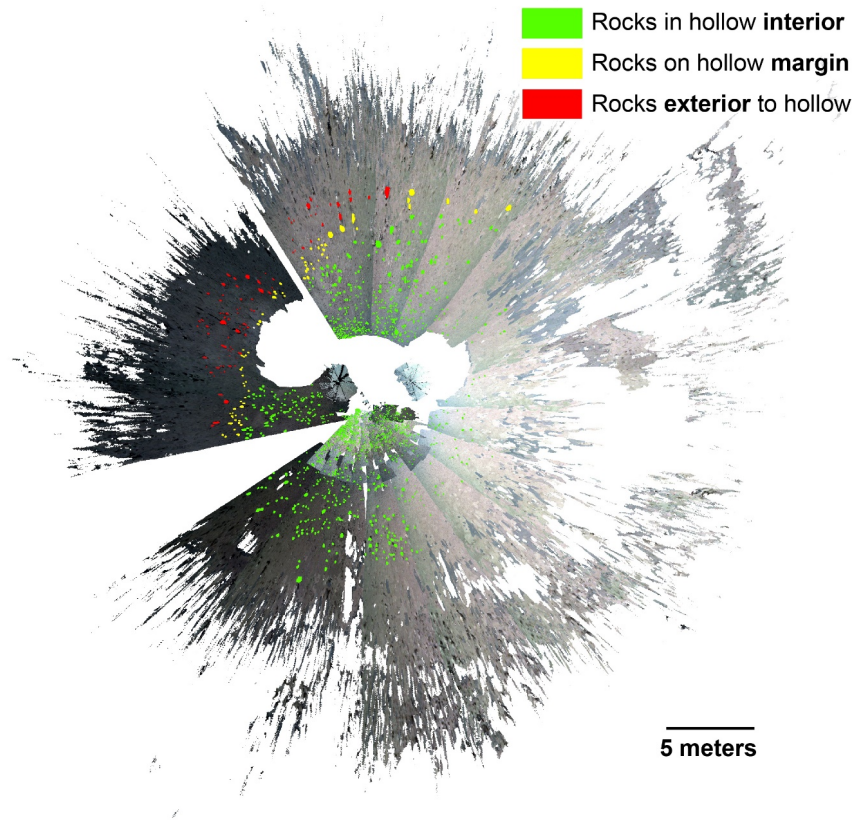


Figure 3. Image of the IDC orthomosaic coverage in and around *Homestead hollow* that covers much of the same area visible in the near- and mid-fields in Figure 2. The current study focuses on rocks within 10 m of the lander and included rocks across a broad swath of the hollow interior (green), within ~1 meter of the margin to the west of the north side of the hollow (yellow, see Figure 2), and outside of the hollow within a few meters of rim to the west and north of the lander (red).

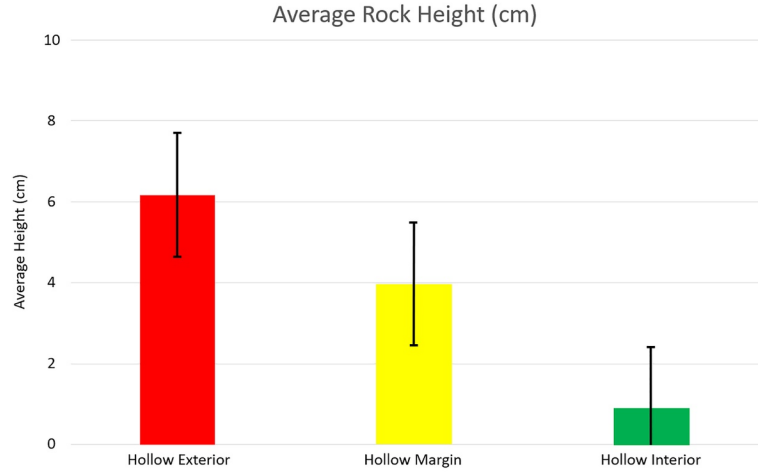


Figure 4. Average height of rocks around the exterior, margin, and interior of Homestead hollow are 6 cm, 4 cm, and 1 cm, respectively. All rocks measured in the DEM are included in the average and the standard error is indicated (standard deviation $N/\text{square root of } N$) that indicates the relative differences in rock height between the three areas are significant (especially between the exterior and interior). Because the rocks around the exterior and margin are more exposed based on their greater size and relative relief, their values are emphasized in consideration of the average amount of eolian stripping that has occurred outside the hollow (Golombek, Warner et al, 2020; Grant et al., 2020; Warner, Grant, et al., 2020) and how much rock fragments may remain embedded in the remnant ejecta.

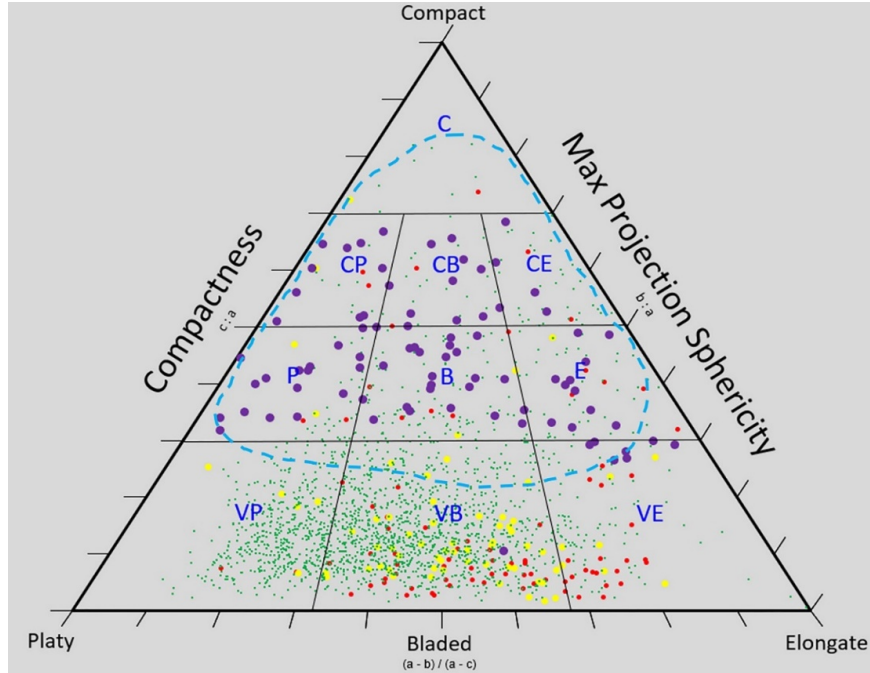


Figure 5. Form factor of basalt rocks in and around the *InSight* lander in *Homestead hollow*. The shape of *InSight* fragments within (green dots), around (yellow dots), and outside (red dots) the hollow plot as mostly platy, bladed, and elongate, whereas the blue dashed line indicates the data cloud for the vast majority of the basalt rocks in ejecta at Lonar crater (Kumar et al., 2014) that is similar to that for basalt rocks in other terrestrial environments (e.g., Ehlmann et al., 2008; Craddock and Golombek, 2016). Purple dots plot the shape of fragments outside the hollow when it is assumed that the rocks remain embedded 10 cm in the remnant ejecta deposit and are generally similar to the shape of basalt fragments defined in terrestrial studies if fully exposed. Field names with abbreviations are: C - compact, CP - compact platy, CB - compact bladed, CE - compact elongated, P - platy, B - bladed, E - elongate, VP - very platy, VB - very bladed, and VE - very elongated. Note that the extreme shapes of Lonar fragments (VP, VB, and VE) are fewer than other shapes.

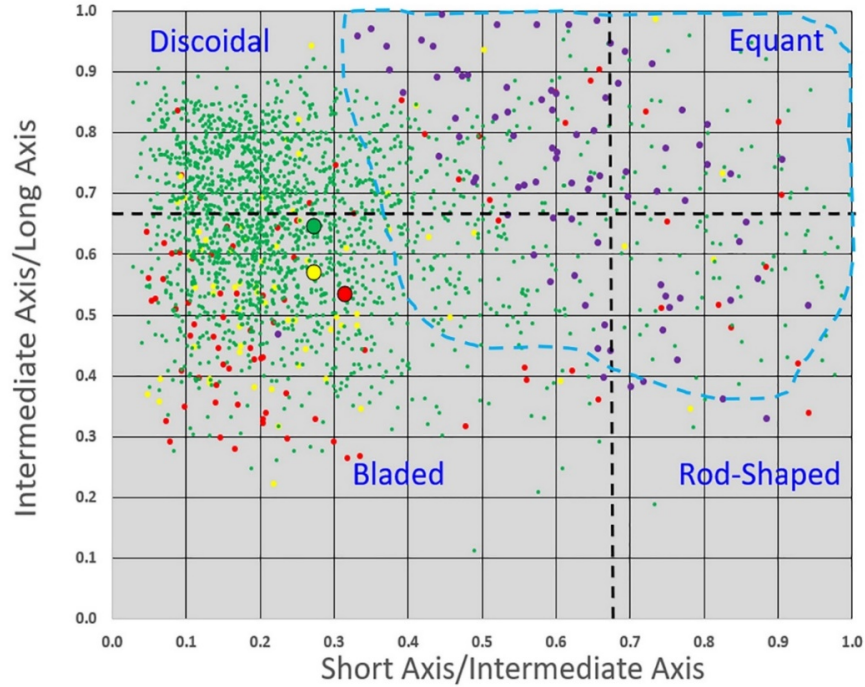


Figure 6. Plot of fragment shape as defined by the ratio of the intermediate to short axis versus the short to intermediate axis after Zingg (1935). There is significant scatter in the data, but the bulk of fragments inside the hollow (green dots) plot near the boundary between discoidal and bladed shapes, whereas fragments along the margin (yellow dots) and outside (red dots) are somewhat more bladed in shape. The large red, yellow, and green dots mark the average of the rocks on the exterior, margin, and interior of the hollow, respectively, and highlight the general similarity in rock shape in and around the hollow. The blue dashed line encompasses the data cloud for the vast majority of basalt ejecta fragments at Lonar crater (Kumar et al., 2014) that is similar to that for basalt rocks in other terrestrial environments (e.g., Ehlmann et al., 2008; Craddock and Golombek, 2016) and are mostly equant (34%) with lesser, but significant disc-, rod- (28%), and blade-shapes (10%). Purple dots are fragments outside the hollow when it is assumed that the rocks remain embedded 10 cm in the surface and are generally similar to the shape of basalt fragments noted in terrestrial studies.

Degradation at the *InSight* Landing Site, *Homestead Hollow*, Mars: Constraints from Rock Heights and Shapes

J. A. Grant¹, S. A. Wilson¹, M. Golombek², A. Trussell^{2,3}, N. H. Warner⁴, N. Williams², C. M. Weitz⁵, H. Abarca², R. Deen²

¹Center for Earth and Planetary Studies, National Air and Space Museum, Smithsonian Institution, 6th at Independence SW, Washington, DC, 20560 ORCID: <https://orcid.org/0000-0001-8276-1281>

²Jet Propulsion Laboratory, California Institute of Technology, Pasadena, CA,

³California Institute of Technology, Pasadena, CA,

⁴SUNY Geneseo, Department of Geological Sciences, 1 College Circle, Geneseo, NY 14454

⁵Planetary Science Institute, 1700 East Fort Lowell, Tucson, AZ, 85719

Submitted to Earth and Space Science 7/29/21

Abstract: Rock heights and three-dimensional shapes around the *InSight* lander in *Homestead hollow*, Mars, provide new constraints on modification of the degraded 27 m in diameter impact crater and are a tool for characterizing degradation on regolith-covered lava plains on Mars. Decreasing average rock height and increasing percentage of fragments where height comprises the short axis from outside to within the hollow supports significant ejecta deflation accompanied by infilling of the interior. Rock relief outside the hollow is compared with expectations of pristine ejecta thickness and indicates up to ~40 cm of near-rim early deflation (decreasing to a few cm out to one diameter) can account for the predicted eolian component of infilling and that other eolian infilling sources are not required. Scattered rocks in the hollow are ejecta from subsequent nearby impacts and their mostly buried expression is consistent with subsequent long-term degradation estimated to be 10^{-4} m/Myr. Basalt rock shapes at *InSight* are likely similar to basalt rock shapes on Earth, but appear more platy, bladed, and elongate in a triangular form factor plot and more discoidal and bladed in an axes ratio plot. Nevertheless, addition of 10 cm to near rim rock heights to account for continued partial embedding in ejecta would result in rock shapes quite similar to terrestrial rocks. Consistency between degradation estimates based on current rock relief and rock shape after accounting for partial embedding in ejecta indicates up to ~30-40 cm early (~0.1 Ga) near-rim deflation was followed by much lesser long-term degradation.

Key Points

Rock heights and shapes at *Homestead hollow* indicate early transport of deflated ejecta sediments can account for infilling of the crater.

Near-rim rock heights and shapes relative to the expected original versus remnant ejecta thickness indicates ~40 cm deflation occurred.

Continued exposure of later arriving, small ejecta rocks in the hollow supports very low estimates of degradation over most hollow history.

1. Introduction

The *InSight* mission (Interior Exploration using Seismic Investigations, Geodesy, and Heat Transport) to Mars landed November 2018 in western Elysium Planitia at 4.502°N, 135.623°E on a regolith-covered, Early Amazonian basaltic lava plain capped by ~3 m of impact-formed regolith (Banerdt et al., 2020; Golombek, Williams et al., 2020; Golombek, Warner et al., 2020). The lander is within a highly degraded, ~400-700 Myr old, ~27 m-diameter impact crater dubbed “*Homestead hollow*” (Golombek, Warner et al., 2020; Grant et al., 2020; Warner, Grant et al., 2020). The present form of the hollow (Fig. 1) contrasts with its predicted pristine morphology: the original ~0.7 m high rim and ~3-4 m depth has been reduced to a subtle depression only 0.3 m deep. Corresponding estimates of hollow infilling are between 3-4 m (Grant et al., 2020; Warner, Grant, et al., 2020). The surface of the interior of the hollow is characterized by relatively fewer/smaller rock fragments with respect to the margin and near-rim of the exterior (Fig. 2), though there are ~3X more rocks in an area dubbed “*Rocky Field*” on the western interior floor relative to the eastern interior floor (Figs. 1 and 2).

Rocks at *InSight* are basaltic in composition and likely of volcanic lava origin based on: (1) relative proximity to north-south trending wrinkle ridges (Golombek et al., 2018); (2) the presence of degraded lobate flow margins in the region (Golombek et al., 2018); (3) occurrence of platy and ridged surface textures and possible lava inflation plateaus and volcanic vents (Pan et al., 2020); (4) rocks with a fairly uniformly fine-grained aphanitic texture (Golombek, Warner et al., 2020); (6) the absence of any observable sedimentary structures in rocks at the landing site; and (7) evidence that the regional Hesperian transition unit around the lander (Tanaka et al., 2014) experienced an Early Amazonian-aged resurfacing event linked to regionally occurring late volcanism (Warner et al., 2017).

Prior studies concluded that hollow degradation was dominated by eolian and mass wasting processes with lesser impact contributions that stripped and lowered the near-rim and ejecta, resulting in nearly complete infilling of the crater interior and burial of any rocks lining the hollow (Golombek, Warner et al., 2020; Grant et al., 2020; Warner, Grant, et al., 2020). Early degradation of the hollow was relatively more rapid and dominated by deflation of fines from the ejecta, some of which were transported downwind and infilled the crater, and was accompanied by mass-wasting along the crater wall. Early degradation continued until coarser fragments created a surface lag on the ejecta and/or sufficient relief around partially exposed rocks created a boundary layer that precluded further stripping while accumulating eolian fill stabilized the walls of the hollow (Grant et al., 2020; Warner, Grant, et al., 2020). Comparisons made using orbital data covering nearby, similar-sized craters in varying stages of degradation (Sweeney et al., 2018; Warner, Grant, et al., 2020) revealed that

Homestead hollow assumed something close to its present form within the first 0.05-0.1 Ga after formation (Grant et al., 2020; Warner, Grant, et al., 2020a). At least some rocks visible in the hollow (e.g., *Rocky Field* on the western side; see Golombek, Warner et al, 2020) are likely related to ejecta from subsequent, nearby impacts, and are therefore not associated with hollow formation: their continued partial exposure highlights evidence for very slow modification that occurred over most of the history of the hollow (Grant et al., 2020; Warner, Grant, et al., 2020). The cumulative result of hollow degradation is characterized primarily by an increase in the number and relative relief of rocks along the margin and exterior of the hollow relative to the filled interior (Fig. 2), and there is no significant topographic transition between the two areas (Warner, Grant, et al., 2020). Nevertheless, the relative relief and shapes of rocks in and around the hollow has not been quantified, and thus possible implications for the amount of exterior stripping and accompanying infilling relative to mass wasting or direct infilling related to ejecta from later impacts are not yet well-defined.

Rock height (vertical measurement of the rock above the adjacent local surface) and three-dimensional shape (various comparisons between the short, intermediate and long axes of a rock) are important parameters used to assess the varying amount and number of geomorphic processes affecting a landscape over time and help identify where erosion dominates over burial and/or help to identify locales where new materials may have been introduced as infilling deposits (Fig. 2).

Rock shape can also be used to help identify the processes and intensity of degradation processes responsible for the characteristics of a rock population, thereby informing (or constraining) which processes have been active and how they may have varied with location over time. A number of studies have examined the two- and three-dimensional shape of rocks (i.e., using either two or three of the principal axes of a rock) on the Earth and Mars. Two-dimensional rock shape characterization can focus on sphericity (Corey, 1949), angularity (Krumbein, 1941) or other characteristics of a rock and is often applied to rocks on Mars where information on all three principal rock axes is precluded by lack of accurate height information (e.g., Garvin et al., 1981; Yingst et al., 2007, 2008, 2010, 2013; Craddock and Golombek, 2016). Three-dimensional evaluation of rock shapes requires accurate measure of all dimensions and can include various ratios or relations between the long, intermediate, and short axes of a rock (e.g., Zingg, 1935; Sneed and Folk, 1958). These relationships are used to characterize rocks as more rounded (compact or equant), disc-shaped, bladed, or elongate (rod). As general examples, Graham and Midgley (2000) showed that three-dimensional rock form is a discriminator between scree, moraine, and frost-shattered deposits. Three-dimensional shape characteristics for terrestrial basalt rocks in a wide range of geologic and weathering environments, including impact, however, show little variability (e.g., Craddock and Golombek, 2016; Ehlmann et al., 2008; Kumar et al., 2014), likely a reflection of control by cooling fractures on how the rocks break (Craddock and Golombek, 2016).

Three-dimensional information related to rock axes at *InSight* is available via processing of stereo images acquired by the lander, enabling direct comparison of rock shapes on Mars to those associated with basalt rocks on the Earth.

Our analysis of variations in the height and shape of basalt rocks around the *InSight* lander can provide additional constraints on geomorphic processes active at the landing site over time to further constrain the responsible processes, their timing, and amount that resulted in hollow degradation. For example, variations in rock height together with information of degradation processes can quantify differences in relief from outside to within the hollow that relates to regions of net erosion versus deposition. Moreover, the relief on rock fragments in ejecta around the hollow, where stripping likely predominates, can be equated to the amount of surface lowering that has occurred when coupled with expectations of the pristine thickness and nature of the deposit. We also explore whether there are significant differences in three-dimensional rock shapes at *InSight* relative to the more uniform shapes observed in terrestrial basalt rocks in a range of environments (e.g., Ehlmann et al., 2008; Kumar et al., 2014; Craddock and Golombek, 2016) and examine how differences in shape may relate to their immediate setting and/or formation and modification of the hollow. For example, the observed versus expected form of the basalt rock fragments outside the hollow coupled with rock relief and expectations of the pristine ejecta thickness can help to predict the degree to which rocks remain embedded in the regolith versus being fully exposed on the surface, further informing the amount of stripping that has occurred. We focus on comparison of shape parameters for the basalt rocks at *Homestead hollow* to shape parameters for basalt rocks in the ejecta deposit at the simple-structure Lonar impact crater, in India (Kumar et al., 2014) to minimize any unlikely, minor uncertainties in interpretation related to differences geologic setting. Our approach helps detail where and how much degradation occurred at the *InSight* landing site, and whether processes occurring locally on and within the hollow can account for the current degraded appearance or whether additional sediments from more distant sources are also required. The approach provides a template that can be used to constrain degradation occurring on widespread, broadly similar volcanic surfaces (e.g., Grant et al., 2004, 2020; Tanaka et al., 2014; Warner, Schuyler, et al., 2020) emplaced over latter portions of Mars history.

1. Measuring Rock Dimensions

The orthogonal dimensions (minimum and maximum horizontal together with height) of rocks around the *InSight* lander were measured from an orthomosaic digital elevation model (DEM) covering much of the nearfield surrounding the lander. Image mosaics of the surface surrounding the landing site were acquired using the arm-mounted Instrument Deployment Camera (IDC, angular resolution of 0.82 mrad/pixel at the center of the image, see Maki et al., 2018). A nearly complete panorama was taken of the landscape around the lander and consists of 283 IDC stereo images (Fig. 2). These images were used to create the orthoimage and DEM of the local environment (Fig. 3). As summarized

from Golombek et al. (2021), IDC image resolution varied from 0.12 cm/pixel to 2.8 cm/pixel with increasing range and the DEM has elevation postings every 5 mm. The panorama orthomosaic was bundle adjusted (Abarca et al., 2019), except for the west region, which is separate from the rest of the panorama (Figs. 2 and 3). Error in stereo coordinates is the result of uncertainty in the robotic arm position and stereo processing errors. Nevertheless, pre-launch tests of the surface in front of the lander had a mean horizontal accuracy of 11 mm, a mean absolute vertical accuracy of 6.5 mm, and mean relative vertical accuracy of 5 mm. After landing, 56 images taken in front of the lander on sol 12 and had a spatial accuracy between adjacent stereo frames of 1.9 mm overall with a maximum error between frames of 4 mm. Images further from the lander, including horizon images, were bundle adjusted to those close to the lander. The error within each stereo pair is characterized by the stereo range error (Maki et al., 2018) of the IDC camera, and range error in the DEM increases from <1 cm to ~13 cm at a distance of 10 m from the lander. Spatial uncertainties in the orthomosaic of <4 mm in the workspace to <1 cm at 10 m distance do not have an appreciable effect on derived rock sizes because they are based on relative measurements of rocks over small distance within the orthomosaic and the spatial uncertainties are smaller than that associated with the overall orthomosaic. Golombek et al. (2021) further estimated that the IDC pixel-scale is 0.5 cm at 5 m distance and that 80-95% of the rocks in the DEM down to 0.01 m diameter could be counted out to 10 m. Finally, it is unlikely that a significant number of small rock fragments are undercounted along the hollow margin and exterior as a result of shadowing by larger blocks because of the height of the IDC during imaging (above the lander deck) and the limited range of the measurements. With these points in mind, rock fragments >1 cm were measured within 10 m of the lander that covers a significant portion of the hollow interior, the hollow margin to the west-north and nearest few meters of the hollow exterior to the west-north (Fig. 3).

For the horizontal dimensions of the rock fragments in and around the hollow, we utilized a population of 2,034 rock fragments examined by Golombek et al. (2021) that characterized the rock size-frequency distribution. As summarized from Golombek et al. (2021), horizontal rock dimensions were made by digitizing polygonal outlines of visible rocks in the orthomosaic in ArcGIS. A convex hull was calculated providing minimum and maximum (non-vertical) axes enclosing a rock. The minimum axis is calculated as the shortest distance between any 2 vertices of the minimum bounding polygon while the maximum axis is calculated as the longest distance between any 2 vertices of the minimum bounding polygon. These measurements are exactly horizontal with no elevation information, yielding the small and large axes for each rock fragment. To measure the height of each fragment, we used the same dataset of 2,034 rocks noted above (Golombek et al. 2021), but removed rocks that were not entirely covered by the 5 mm DEM. The height (Z) of each rock was derived from the 5mm DEM (with 0.5-1 mm vertical precision) using the Add Surface Information plug-in in ArcGIS which calculated the difference between the maximum

(Z_MAX) and minimum (Z_MIN) values for each fragment (as mapped by the bounding polygon). Measurements are rounded to the nearest centimeter to maximize confidence in the estimated dimensions. Our final database of rock dimensions includes 2,004 rocks (Fig. 3), distributed in three areas: A) the hollow interior (n=1,850, including *Rocky Field* and more rock-free portions of the interior); B) the hollow margin (n=68) defined as rocks within ~1 m of the zone of increased rock density relative to the hollow interior (Fig. 2); and C) the hollow exterior (n=85) within a few meters beyond the hollow margin to the west-northwest of the lander. Fragment dimensions (minimum horizontal, maximum horizontal, and height) were used to evaluate any systematic changes in rock height or shape within the hollow interior, along the hollow margin, or exterior to the hollow. Our initial assumption is that the rock sizes lining the interior and along the wall (margin) and near-rim should all be generally similar given they are the last materials being excavated during crater formation (average rock size should decrease with increasing distance from the rim). It is likely, however, that increasing thickness of fill from the margin towards the hollow interior results in at least partial burial of many rocks emplaced during the impact-formation of the crater.

1. Measuring Rock Shape

Rock shapes for fragments in and around the *Homestead hollow* were derived using commonly used calculations (Sneed and Folk, 1958) for maximum projection sphericity (φ), deviation from compactness (D), and form factor (F):

$$\varphi = \sqrt[3]{\frac{S^2}{LI}} \quad (1)$$

$$D = \frac{S}{L} \quad (2)$$

$$F = \frac{L-I}{L-S} \quad (3)$$

Where L , I , and S correspond to the *long*, *intermediate*, and *short* axes of each rock fragment, respectively. Ratios of the length of each axis are then plotted to obtain the form factor using the equations (1)-(3) in the TRI-PLOT excel program published by Graham and Midgley (2000) to constrain the distribution of compact, platy, bladed, and elongate fragments. In addition, the ratios of the rock fragment intermediate to long axis versus fragment short to intermediate axis was plotted separately (after Zingg, 1935) to characterize whether fragments are more equant, discoidal, bladed, or rod-shaped relative to expectations from studies of terrestrial basalt rocks (e.g., Ehlmann et al., 2008; Kumar et al., 2014; Craddock and Golombek, 2016).

1. Results

Rock heights on the exterior, margin, and interior of the hollow (Fig. 3) are often the shortest measured axis (height is the short axis 78% of exterior rocks, 91% of margin rocks, and 97% of interior rocks) (Table 1, see also Grant et al. (2021) data repository for additional details). For the exterior of the hollow, the 10 tallest rocks stand between 23-30 cm in exposed relief (five largest rocks

are >28 cm in height), and 22% of the rocks are >10 cm tall. The 10 tallest rocks along the hollow margin stand between 4-33 cm in exposed relief (five largest rocks are 25-34 cm in height), with 10% of the rocks > 10 cm tall. In the hollow interior, the 10 tallest rocks stand between 14-26 cm in exposed relief, but less than 1% of the rocks are > 10 cm tall (Table 1). The decrease in rock height from the exterior to the interior of the hollow is also apparent in the overall average height of rocks within each zone, with rocks outside the hollow, around the hollow margin, and inside the hollow measuring 6 cm, 4 cm, and 1 cm tall, respectively (Table 1, Fig. 4). The standard error associated with the height in each zone indicates that the differences are significant (Fig. 4), especially between the exterior and the interior of the hollow. To evaluate whether the difference in the height of rocks outside versus within the hollow is related to larger versus smaller rocks within the hollow, height values were normalized by dividing the rock height by the average of the width and length. Resultant values for the exterior rocks are 0.42 (0.65 standard deviation) versus 0.27 (0.34 standard deviation) and 0.25 (0.42 standard deviation) for the margin and interior rocks, respectively. These values are consistent with a wide range in rock sizes in all three areas, but that are generally higher and more exposed around the exterior of the hollow.

With the above in mind, study of rock shape focused on rock fragments on the exterior and margin of the hollow (see also Grant et al. (2021) data repository for additional details) because they are more exposed, consistent with predictions (Golombek, Warner, et al., 2020; Grant et al., 2020; Warner, Grant, et al., 2020). For exterior fragments, the maximum projection sphericity (equation 1) ranges from 0.11 to 0.87 with a mean of 0.35 (0.21 standard deviation) and from 0.10 to 0.81 with a mean of 0.33 (0.15 standard deviation) for the margin (Table 1). The deviation from compactness (equation 2) is 0.02 to 0.74 with a mean of 0.18 (0.18 standard deviation) for the exterior and from 0.02 to 0.73 with a mean of 0.16 (0.13 standard deviation) for the margin (Table 1). The form factor (equation 3) for the exterior ranges from 0.18 to 0.97 with a mean of 0.57 (0.18 standard deviation) for the exterior and from 0.05 to 0.90 with a mean of 0.52 (0.17 standard deviation) for the margin (Table 1). By comparison, basalt rock fragments in the ejecta deposit at Lonar crater have a maximum projection sphericity 0.11 to 1.0 with a mean of 0.72, the deviation from compactness is 0.18 to 1.0 with a mean of 0.53, and the form factor ranges from 0 to 1 with a mean of 0.56 (Table 1). As such, the most similar shape parameter between the rock fragments at *InSight* and in the ejecta at Lonar crater is the form factor. When plotted (Sneed and Folk, 1958; Zingg, 1935) and compared to the shape of basaltic fragments in ejecta at Lonar crater (Kumar et al., 2014) large differences can be seen (Figs. 5 and 6): the rock fragments in all three zones in and around the hollow at *InSight* appear significantly more platy, bladed, and elongate in the triangular form factor plot (Fig. 5) and the bulk of fragments inside the hollow are discoidal and bladed and rocks along the hollow margin and exterior are more bladed in the axes ratio plot (Fig. 6). By contrast, the rock fragments at Lonar are mostly compact, compact

platy, compact bladed, compact elongated, platy, bladed, and elongate in the triangular form factor plot (Fig. 5), whereas ejecta fragments at Lonar are mostly equant with lesser, but significant disc- and blade-shaped fragments in the axes ratio plot (Fig. 6). Although Lonar is a relatively fresh impact crater where rocks have been subjected to more rapidly weathering versus the very degraded appearance of *Homestead hollow*, evaluation of basalt rock shapes from diverse geologic and weathering environments on Earth indicates there should be little effect on expected rocks shapes (Craddock and Golombek, 2016).

1. Discussion

The greater rock height outside the hollow is confirmed after normalizing for possible variations in overall rock size that indicates differences are not solely the result of larger versus smaller rocks around and within the hollow (Fig. 4). This observation coupled with an increasing percentage of rocks where height corresponds to the measured short axis from outside to around to within the hollow supports the greater exposure of rocks on the near rim relative to the interior and is consistent with inferred degradation of the hollow dominated by stripping fines from the exposed ejecta deposit accompanied by downwind deposition and infilling of the hollow (Golombek, Warner et al., 2020; Grant et al., 2020; Warner, Grant, et al., 2020). Reasonable expectations of relative rocks sizes around and within the pristine crater, however, suggest that the difference in rock height between the exterior and interior of the hollow is not a simple reflection of the difference between the total of exterior stripping versus interior infilling that has occurred.

Examination of the ejecta remnants around *Homestead hollow* and other fresh, nearby small craters reveals only a few meter-scale rocks (Golombek, Williams et al., 2020; Warner et al., 2017) and implies those lining the original floor and walls of the hollow are of a similar scale and are of a lesser size than the depth of fill. This contention is supported by the paucity of rocks observed in HiRISE images of craters <30-40 m in the vicinity of the landing site (Warner et al., 2017) and the expectation that the original 3-4 m depth of the hollow largely limited impact excavation to the pre-existing impact regolith (Banerdt et al., 2020; Golombek, Williams et al., 2020; Golombek, Warner et al., 2020) rather than excavating larger rocks from more competent material below that could yield larger rocks (that result in Rocky Ejecta Craters or RECs, see Warner, Grant, et al., 2020). In addition, the local regolith has locally experienced approximately three impact events that would be responsible for breaking any large blocks into smaller fragments (Charalambous et al., 2020; Golombek et al., 2018, 2021). However, even if the hollow-forming impact occurred into bedrock, the maximum expected fragment size of 0.9-2.8 m (based on the relation between crater size and largest associated rock described in Moore (1971) makes it very likely that rocks lining the original hollow floor are buried beneath the fill (Grant et al., 2020). Hence, the difference in rock height between the exterior and interior of the hollow is only a partial reflection of the deflation versus infilling that has occurred. More likely, the generally smaller size and distribution of

exposed interior rocks (e.g., forming *Rocky Field*) is consistent with later arriving ejecta fragments from nearby impacts as described in Grant et al. (2020) that have since been partially buried.

Nevertheless, consideration of the rock height/exposure on the near-rim relative to expected characteristics of the pristine ejecta can be used to understand the amount of deflation that has occurred there. To start, the approximate pristine ejecta thickness around the hollow can be estimated using:

$$E_t = 0.14R_t^{0.74}(r/R_t)^{-3.0} \quad (4)$$

Where the ejecta deposit (E_t , measured in meters) can be related to the transient crater radius R_t (where the transient crater diameter D_t is $0.84D$ (D is the final diameter)) and radial distance r from the crater rim, where $r > R_t$ (McGetchin et al., 1973). Predicted ejecta thickness around the pristine *Homestead hollow* ranges from ~50 cm at the rim to around 30 cm three meters outside the rim, 20 cm five meters beyond the rim, 10 cm at 1 radius, and only a couple of cm at 1 D range.

Based on analogy with ejecta deposits around Meteor Crater, AZ, (Grant and Schultz, 1993) and Lonar crater (Kumar et al., 2014), the pristine ejecta deposit around *Homestead hollow* likely graded from more clast rich, perhaps clast supported, to matrix rich, perhaps matrix-supported deposit with increasing radial distance from the rim. Although thinner, ejecta further from the rim was likely characterized by fewer large fragments and more abundant fines, and may have supplied relatively more sediment (i.e., per unit volume) for transport due to a lesser abundance of lag or surface armoring fragments. Moreover, the multiple impact gardening of the regolith into which *Homestead hollow* formed would have produced abundant sand-sized material at the expense of fewer larger rocks in accordance with expectations from fragmentation during three impact events (Golombek, Charalambous et al., 2020; Golombek et al., 2018, Golombek et al., 2021). Finally, the numerous rocks that are exposed around the margin and exterior of *Homestead hollow* implies the hollow-forming impact did not occur into pre-existing fines filling an older crater, in which case even more fines and fewer clasts would be expected (Grant et al., 2020). In any of these situations, variable numbers of relatively large (10s of cm up to ~1 m) fragments would likely be present, but more common/numerous in the vicinity of the rim-crest.

Hence, the pristine ejecta deposit around the hollow was likely characterized by a wide range of fragment sizes, but with a paucity of large fragments standing in significant relief. The pristine surface would have been in disequilibrium with regional geomorphic thresholds (Grant et al., 2020; Warner, Grant, et al., 2020) and susceptible to deflation that would have continued until fragments too large to be transported accumulated as an armoring lag and/or increasing rock relief created boundary layer that precluded further eolian transport (Grant et al., 2020). With these points in mind, differing amounts of amount of eolian deflation from the ejecta around the hollow can be approximated and compared to the volume associated with fill inside the hollow.

The volume of fill within the 27 m-diameter hollow can be constrained to first order using an original depth of ~3-4 m that is now 0.3 m post-infilling (Warner, Grant, et al., 2020) and yields a total fill volume of ~500-700 m³. If on order of 60% of the infill is due to diffusional infilling from around the hollow and 40% is due to eolian infilling (based on evaluation of ~100 m-diameter craters in the region, Sweeney et al., 2018) then the eolian contribution to infilling is ~200-280 m³. The small size and limited pristine depth of *Homestead hollow* suggests steep slopes facilitating diffusional infilling were of limited extent and would have been stabilized by increasing accumulation of eolian infill. Hence, the actual eolian component to infilling may have been somewhat greater than 40%.

It is unlikely that the 6 cm greater average relief of fragments on the near-rim of the hollow reflects a uniform amount of ejecta stripping from the entire deposit given the greater exposed relief on many of the near-rim rocks (as compared to the likely appearance of the pristine deposit) and the limited thickness of ejecta beyond about 1R from the rim. (Golombek, Warner et al, 2020; Grant et al., 2020; Warner, Grant, et al., 2020). Despite that, an average of 6 cm deflation to a distance of 1D from the rim would supply ~300 m³ of sediment, close to what is required if all the all of the fill was eolian. Prevailing, reversing north-west-southeast winds (Spiga et al., 2018), however, would cause a significant fraction of sediment to be transported downrange and bypass the hollow. If half of the deflated sediment was blown back into the hollow, the volume contributing to infilling could be ~150 m³ and somewhat less than the lower end estimate of a 40% eolian contribution to the total fill volume. A more realistic estimate of the eolian erosion from the ejecta might be obtained from the relief on exposed near-rim rocks, given most were likely buried or expressed limited relief in the pristine deposit, coupled with use of a decreasing amount of deflation with increasing range that better reflects the decreasing thickness of ejecta with increasing distance from the rim. The maximum relief of rocks around the hollow is ~0.3 m as measured in the DEM and there are a few instances of rock relief as large as 0.4 m (First Rock, ~20 m distance) and 0.5 m (Hanging Rock, ~21 m distance) beyond the limit of the DEM (Golombek, Williams et al, 2020; 2021). Based on those rock heights and estimates of pristine ejecta thickness that decrease outside the rim, deflation of 0.4 m to a range of 3 m beyond the rim, 0.25 m between 3-5 m beyond the rim, 0.13 m 5-15 m beyond the rim, and 0.03 m from 15-27 m beyond the rim yields a sediment volume of ~440 m³. While this exceeds the volume of the expected eolian contribution to hollow infilling, it is a reasonable match if ~50% is blown back into the crater by the prevailing winds and the remaining deflated sediments bypassed the hollow. If the volume of fill in the hollow is on the lower end of estimates and/or a slightly larger percentage of deflated sediments are blown back into the crater, then eolian contributions could approach 50% or slightly more, but likely would not comprise an overwhelming fraction of the infilling sediments.

Rock shapes at *Homestead hollow* provide an independent check on whether our deflation estimates are realistic. In contrast to the expectation of mostly

compact, compact platy, compact bladed, compact elongated, platy, bladed, and elongate rocks (Fig. 5) or mostly equant ($\sim 1/3$ of the total) with lesser, disc- and blade-shaped fragments (Fig. 6) at *InSight* based on comparison to rocks at Lunar crater (and elsewhere, Ehlmann et al., 2008; Kumar et al., 2014; Craddock and Golombek, 2016) there is a preponderance of platy, bladed, and elongate rocks. Further, at *Homestead hollow*, the average maximum projection sphericity (equation 1) of 0.35 and average deviation from compactness (equation 2) of just under 0.2 are well below the average of 0.72 and 0.53, respectively, of fragments measured at Lunar crater. However, the form factor (equation 3) for fragments at *InSight* averages 0.5-0.6 and is comparable to the average of 0.56 observed at Lunar and may hold a clue to understanding the cause of other differences.

Possible reasons for apparent differences in rock shape parameters at *InSight* include: A) error in measurements made in the direction viewed from the lander if the fragment profile precludes accurate measure of dimensions; and/or B) the partially buried nature of the *InSight* fragments (especially inside the hollow) leads to underestimate of the axis associated with rock height. The former can be ruled out because there is no systematic change in the shape parameters with increasing distance from the lander when viewed more obliquely.

For the second possibility, the partially embedded appearance of many of the near-rim rocks, and more buried appearance of rocks within the hollow, suggests that the actual rock heights are being underestimated. The predominance of rock height as the smallest fragment axis, provides support for this statement. For example, height acts as the short axis for a large majority (78%) of the fragments on the near-rim and suggests that underestimation of rock height is skewing the shape analyses. Equations (1) and (2) emphasize the smallest rock axis in the numerator that can lead to lesser estimated values of maximum projection sphericity and deviation from compactness. By contrast, the form factor includes the smallest axis of each fragment as a difference in the denominator and could have a lesser impact on the calculated values that appear to better match what is seen in the *InSight* versus terrestrial rocks.

In order to consider the effects of underestimating rock height on derived rock shapes, we recalculated shape parameters and plots after addition of relief to rocks on the near-rim to account for their partially embedded appearance. We focused on fragments around the exterior of the hollow because they are the best exposed (based on greater rock relief and somewhat lesser percentage of measured height as the short fragment axis) and made comparisons to the maximum estimated thickness of the original ejecta deposit.

The estimated 30-50 cm original thickness of pristine ejecta within a few meters of the hollow rim (covered by the DEM) coupled with the ~ 30 cm relief on some partially embedded fragments in the same zone makes it reasonable that an average ~ 10 cm ejecta (plus/minus) buries the base of many fragments. Accordingly, 10 cm was added to the height of each rock on the exterior of the hollow as an estimate for the rock fraction that remains embedded/buried and

resultant revised heights were used in recalculation of shape parameters. The revised average values for maximum projection sphericity are 0.65 (0.09 standard deviation, range between 0.29 and 0.85), compactness is 0.45 (0.11 standard deviation, range between 0.11 and 0.68), and form factor is 0.49 (0.26 standard deviation, range 0.01 and 0.95), all much closer to the corresponding values of 0.72, 0.53, and 0.56 for ejecta fragments at Lonar crater, respectively. The resultant updated data cloud for exterior rocks including the revised heights are shown in the TRI-PLOT (Sneed and Folk, 1958) and mostly superposes the data cloud for rocks in the ejecta at Lonar crater. Results suggest that continued ~10 cm embedding of the near-rim exterior rocks can account for most of the observed differences in rock shape between *Homestead hollow* and what is expected from basalt rocks at Lonar crater (Kumar et al., 2014) and in other terrestrial locations (e.g., Ehlmann et al., 2008; Craddock and Golombek, 2016). Hence, ~30 cm or slightly more deflation from the near-rim (decreasing outwards) is supported by greater near-rim rock heights, deflation estimated from the near-rim based on comparison of rock height and original ejecta thickness, and consistency between revised rock relief, estimated original ejecta thickness, and expected rocks shapes.

Interior rocks provide additional clues to the degradation history of the hollow. Rocks inside the hollow average ~1 cm in height and more than >99% are less than 10 cm tall and it is likely that most or all are distal ejecta delivered during nearby impacts (Grant et al., 2020). Those associated with *Rocky Field* were likely emplaced within the first 0.1 Ga of hollow history (Sweeney et al., 2018; Grant et al. 2020; Warner, Grant, et al., 2020). Although the actual size of the interior fragments is uncertain due to their partial burial, the ratio of their height to average width and comparison to average size of more exposed rocks on the rim coupled with likely emplacement as distal ejecta (Grant et al. 2020) suggests most are small and likely less than 10 cm tall. Warner, Grant, et al. (2020) and Grant et al. (2020) estimated initially high degradation rates during the first ~0.1 Ga after hollow formation quickly slowed as surrounding ejecta became armored by a coarse lag and/or increasing surface relief due to around larger rocks created a boundary layer that precluded eolian transport. Degradation rates following this early period were estimated to be 10^{-4} m/Myr for most of the 0.4-0.7 Ga history of the hollow (Sweeney et al., 2018; Warner, Grant, et al. 2020) equating to ~3-6 cm of infilling since emplacement of the fragments forming *Rocky Field*. The likely small size, but continued, limited exposure of the fragments in *Rocky Field* and other interior rocks is consistent with these estimates of very slow degradation over the bulk of hollow history.

Our results provide a new means for constraining hollow degradation that is consistent with prior predictions of modification history. The exposed rock relief and revised rock shapes on the near-rim support deflation of up to 40 cm at the near-rim, decreasing with range, and is a good match with expected eolian contributions of 40% or slightly more to hollow infilling: the remainder of infilling is likely the result of diffusional processes (Sweeney et al. 2018; Warner, Grant, et al., 2020) with only minimal additional infilling contributions associ-

ated with eolian transport from ejecta around later forming craters. Instead, the inventory of deflated ejecta sediment bypassing the hollow likely contributed to eolian bedforms in the vicinity of the landing site (e.g., Golombek, Warner, et al., 2020).

Further, limited hollow infilling via deflation off ejecta around later impacts is consistent with early, more rapid infilling followed by very slow degradation over the bulk of hollow history. Continued exposure of *Rocky Field* and other interior rocks supports this model. Small rocks forming *Rocky Field* were likely emplaced during the first ~ 0.1 Ga after the hollow formed (Grant et al., 2020; Warner et al., 2020) on a surface close to what is observed in the hollow today. And their continued exposure is inconsistent with more significant infilling associated with eolian transport from ejecta around later occurring impacts.

1. Summary

The rocks heights and shapes around and within *Homestead hollow* provide independent evidence regarding degradation over time that are generally consistent with processes inferred from prior studies (Golombek, Warner, et al. 2020; Grant et al., 2020; Warner, Grant, et al., 2020). Decreasing average rock height, decreasing largest (exposed) fragment size, and increasing percentage of fragments where height is the short axis characterize rocks from outside to within the hollow. These observations coupled with evaluation of likely pristine ejecta thickness and properties support net stripping of the ejecta of up to ~ 40 cm in the near-rim and eolian contribution of 40% or slightly more to the inventory of sediments filling of the hollow. Moreover, differences between observed versus expected rock shapes on the exterior of the hollow are found to relate mostly to underestimating rock height as a result of continued ~ 10 cm embedding of near-rim fragments in the remnant ejecta deposit. Recalculation of rock shapes to accommodate an average additional height of ~ 10 cm leads to a close match to expected terrestrial basalt rock shapes Earth (e.g., Ehlmann et al., 2008; Kumar et al., 2014; Craddock and Golombek, 2016) and further constrains near-rim deflation to around ~ 30 cm or slightly more (with an additional ~ 10 cm remaining). Continued exposure of rocks within the hollow (e.g., *Rocky Field*) support estimates of only 10^{-4} m/Myr degradation for most of the 0.4-0.7 Ga history of the hollow (Sweeney et al., 2018; Warner, Grant, et al. 2020). Results suggest that a significant fraction of sediments deflated from the ejecta bypass the hollow via prevailing winds and are likely trapped by local topography, with some contributing to numerous nearby bedforms rather than appreciable infilling of downwind impact structures.

The estimated amount of degradation inferred from rock relief and shape around and within *Homestead hollow* helps to quantify, and is consistent with, both the current and predicted initial appearance of the crater as well as the estimated amount of modification and geomorphic processes it has experienced since formation (Golombek, Warner, et al., 2020; Grant et al., 2020; Warner, Grant, et al., 2020). Because volcanic surfaces of intermediate to young age are widespread on Mars (Tanaka et al., 2014), evaluation of rock heights and shape around small

impact craters can be an important tool for understanding local degradation history

1. Acknowledgements, Samples, Data

We thank the Jet Propulsion Laboratory, Lockheed Martin Space Systems, CNES, and other partner institutions that built and operate the *InSight* lander. A portion of the work was supported by the InSight Project at the Jet Propulsion Laboratory, California Institute of Technology, and under grants 80NSSC18K1625 to J. Grant (includes S. Wilson and C. Weitz) and 80NSSC18K1624 to N. Warner from the National Aeronautics and Space Administration. All data used in the paper is freely accessible at the link provided below in the Data Availability Statement that follows. This is InSight Contribution Number 229.

1. Data Availability Statement

All data used in analyses of rocks at the InSight lander and described in the paper are included in two Microsoft 365 Excel files (and associated readme explanation Word file) and ArcGIS shape files (and associated readme explanation Word file, and orthophoto and DEM) that can be freely accessed and downloaded for viewing at Smithsonian.figshare: <https://doi.org/10.25573/data.15121554>.

1. References

- Abarca, H., Deen, R., Hollins, G., Zamani, P., Maki, J., Tinio, A., et al. (2019). Image and data processing for InSight lander operations and science. *Space Science Reviews*, 215(2), 22. <https://doi.org/10.1007/s11214-019-0587-9>
- Banerdt, W. B., Smrekar, S. E., Banfield, D., Giardini, D., Golombek, M., Johnson, C. L., et al. (2020). Early results from the InSight mission: Mission overview and global seismic activity. *Nature Geosciences*, 13, 183-189. <https://doi.org/10.1038/s41561-020-0544-y>.
- Charalambous, C. (2014). On the evolution of particle fragmentation with applications to planetary surfaces. PhD Thesis, Imperial College London.
- Craddock, R. A., & Golombek, M. P. (2016). Characteristics of terrestrial basaltic rock populations: Implications for Mars lander and rover science and safety. *Icarus*, 274, 50-72. <https://doi.org/10.1016/j.icarus.2016.02.042>.
- Ehlmann, B. L., Viles, H. A., & Bourke, M. C. (2008). Quantitative morphologic analysis of boulder shape and surface texture to infer environmental history: A case study of rock breakdown at the Ephrata Fan, Channeled Scabland, Washington. *Journal of Geophysical Research*, 113, F02012. <https://doi.org/10.1029/2007JF000872>.
- Garvin, J.B., Mouginiis-Mark, P.J., & Head, J.W. (1981). Characterization of rock populations on planetary surfaces: Techniques and a preliminary analysis of Mars and Venus. *Moon Planets*, 24, 355-387.

- Golombek, M. P., Grant, J. A., Crumpler, L. S., Greeley, R., Arvidson, R. E., Bell, J. F., III, et al. (2006). Erosion rates at the Mars Exploration Rover landing sites and long-term climate change on Mars. *Journal of Geophysical Research*, 111. <https://doi.org/10.1029/2006JE002754>.
- Golombek, M., Kipp, D., Warner, N., Daubar, I. J., Fergason, R., Kirk, R. L., et al. (2017). Selection of the InSight landing site. *Space Science Reviews*, 211(1-4), 5–95. <https://doi.org/10.1007/s11214-016-0321-9>.
- Golombek, M. P., Grott, M., Kargl, G., Andrade, J., Marshall, J., Warner, N., et al. (2018). Geology and physical properties investigations by the InSight lander. *Space Science Reviews*, 214, 84. <https://doi.org/10.1007/s11214-018-0512-7>.
- Golombek, M. P., Charalambous, C., Pike, W. T., & Sullivan, R. (2018). The origin of sand on Mars (expanded abstract). *49th Lunar and Planetary Science*, Abstract #2319, Lunar and Planetary Institute, Houston.
- Golombek, M., Williams, N., Warner, N. H., Parker, T., Williams, M. G., Daubar, I., et al. (2020). Location and setting of the Mars *InSight* lander, instruments, and landing site. *Earth and Space Science*, 7, e2020EA001248. <https://doi.org/10.1029/2020EA001248>.
- Golombek, M. P., Warner, N. H., Grant, J. A., Hauber, E., Ansan, V., Weitz, C. M., et al. (2020). Geology of the InSight landing site on Mars: Nature Communications, 11. <https://doi.org/10.1038/s41467-020-14679-1>.
- Golombek, M., Charalambous, C., Pike, W. T., & Sullivan, R. (2020). The origin of sand and dust on Mars: Evidence from the InSight landing site (expanded abstract). *51st Lunar and Planetary Science*, Abstract #2744, Lunar and Planetary Institute, Houston.
- Golombek, M. P., Trussell, A., Williams, N., Charalambous, C., Abarca, H., Warner, N. H., et al. (2021). Rock Size-frequency distribution of the InSight landing site, Mars. *Earth and Space Science*. (in review).
- Graham, D. J., & Midgley, N. G. (2000). Graphical representation of particle shape using triangular diagrams: An Excel spreadsheet method. *Earth Surface Processes and Landforms*, 25(13), 1473 – 1477. [https://doi.org/10.1002/1096-9837\(200012\)25:133.0.CO;2-C](https://doi.org/10.1002/1096-9837(200012)25:133.0.CO;2-C).
- Grant, J. A., & Schultz, P. H. (1993). Erosion of Ejecta at Meteor Crater, Arizona. *Journal of Geophysical Research*, 98, 15,033-15,047.
- Grant, J. A., Arvidson, R. E., Bell, J. F., III, Cabrol, N. A., Carr, M. H., Christensen, P. R., et al. (2004). Surficial deposits at Gusev Crater along Spirit rover traverses. *Science*, 305, 807-810. <https://doi.org/10.1126/science.1099849>.
- Grant, J. A., Warner, N. H., Weitz, C. M., Golombek, M. P., Wilson, S. A., Baker, M., et al. (2020). Degradation of Homestead hollow at the InSight landing site based on the distribution and properties of local deposits. *Journal of Geophysical Research*, 125. <https://doi.org/10.1029/2019JE006350>.

- Grant, J. A., Wilson, S. A., Golombek, M. P., Trussell, A., Warner, N. H., Williams, N., et al. (2021). Data repository for rock dimension data and related plots for fragments around the *InSight* lander, Mars. Smithsonian figshare: see <https://doi.org/10.25573/data.15121554>.
- Senthil Kumar, P., Prasanna Lakshmi, K. J., Krishna, N., Menon, R., Sruthi, U., Keerthi, V. (2014). Impact fragmentation of Lonar Crater, India: Implications for impact cratering processes in basalt. *Journal of Geophysical Research*, 119, 2029–2059. <https://doi.org/10.1002/2013JE004543>.
- Maki, J., Golombek, M. P., Deen, R., Abarca, H., Sorice, C., Goodsall, T., et al. (2018). The color cameras on the InSight lander. *Space Science Reviews*, 214, 105. <https://doi.org/10.1007/s11214-018-0536-z>.
- McGetchin, T. R., Settle, M., & Head J. W. (1973). Radial thickness variation in impact crater ejecta: Implications for lunar basin deposits. *Earth and Planetary Science Letters*, 20, 226-236.
- Melosh, H. J. (1989). *Impact Cratering*, 245 pp., Oxford University Press, New York.
- Moore, H. J. (1971). Large blocks around lunar craters, in *Analysis of Apollo 10 Photography and Visual Observations*. *NASA Special Publication*, SP-232, 26–27.
- Pan, L., Quantin-Nataf, Q., Tauzin, B., Michaut, C., Golombek, M. P., Lognonné, P., et al., et al. (2020). Crust stratigraphy and heterogeneities of the first kilometers at the dichotomy boundary in western Elysium Planitia and implications for InSight lander. *Icarus*, 338. <https://doi.org/10.1016/j.icarus.2019.113511>
- Sneed, E. D., & Folk, R. L. (1958). Pebbles in the lower Colorado River, Texas: A study in particle morphogenesis. *Journal of Geology*, 66(2), 114– 150.
- Spiga, A., Banfield, D., Teanby, N. A., Forget, F., Lucas, A., Kenda, B., et al. (2018). Atmospheric science with *Insight*. *Space Science Reviews*, 214, 109. <https://doi.org/10.1007/s11214-018-0543-0>.
- Sweeney, J., Warner, N. H., Ganti, V., Golombek, M. P., Lamb, M. P., Ferguson, R., & Kirk, R. (2018). Degradation of 100-m-scale rocky ejecta craters at the InSight landing site on Mars and implications for surface processes and erosion rates in the Hesperian and Amazonian. *Journal of Geophysical Research*, 123, 2732. <https://doi.org/10.1029/2018JE005618>.
- Tanaka, K., Skinner, J. A. Jr., Dohm, J. M., Irwin, R. P. III, Kolb, E. J., Fortezzo, C. M., et al., et al. (2014). Geologic map of Mars, United States Geological Survey Science Investigations. *Mappemonde*, 3292.
- Warner, N. H., Golombek, M. P., Sweeney, J., Ferguson, R., Kirk, R., & Schwartz, C., (2017). Near surface stratigraphy and regolith production in southwestern Elysium Planitia, Mars: Implications for Hesperian-Amazonian

terrains and the *InSight* lander mission. *Space Science Reviews*, 211, 147. <https://doi.org/10.1007/s11214-017-0352-x>.

Warner, N. H., Grant, J. A., Wilson, S. A., Golombek, M. P., DeMott, A., Charalambous, C., et al. (2020). An impact crater origin for the InSight landing site at Homestead Hollow: Implications for near surface stratigraphy, surface processes, and erosion rates. *Journal of Geophysical Research*, 125. <https://doi.org/10.1029/2019JE006333>.

Warner, N. H., Schuyler, A. J., Rogers, A. D., Golombek, M. P., Grant, J. A., Wilson, S. A. (2020). Crater morphometry on the mafic floor unit at Jezero crater, Mars: Comparisons to a known basaltic lava plain at the InSight landing site. *Geophysical Research Letters*, 47. <https://doi.org/10.1029/2020GL089607>.

Williams, N., Golombek, M. P., Warner, N. H., Daubar, I. J., Hausmann, R. B., Hauber, E., et al. (2019). Surface alteration from landing InSight on Mars and its implications for shallow regolith structure. *50th Lunar and Planetary Science*, Abstract #2781. *Lunar and Planetary Institute*, Houston.

Yingst, R. A., Haldemann, A. F. C., Biedermann, K. L., & Monhead, A. M. (2007). Quantitative morphology of rocks at the Mars Pathfinder landing site. *Journal of Geophysical Research*, 112, E06002. <https://doi.org/10.1029/2005JE002582>.

Yingst, R. A., Crumpler, L., Farrand, W. H., Li, R., Cabrol, N. A., & Neakrase, L. D. (2008). Morphology and texture of particles along the Spirit rover traverse from sol 450 to sol 745. *Journal of Geophysical Research*, 113, E12S41. <https://doi.org/10.1029/2008JE003179>.

Yingst, R. A., Crumpler, L., Farrand, W. H., & de Souza P. (2010). Constraints on the geologic history of “Home Plate” materials provided by clast morphology and texture. *Journal of Geophysical Research*, 115, E00F13. <https://doi.org/10.1029/2010JE003668>.

Yingst, R. A., Kah, L. C., Palucis, M., Williams, R. M. E., Garvin, J., Bridges, J. C., et al. (2013) Characteristics of pebble- and cobble-sized clasts along the Curiosity rover traverse from Bradbury Landing to Rocknest. *Journal of Geophysical Research*, 118, 2361–2380. <https://doi.org/10.1002/2013JE004435>.

Zingg, T. (1935). Beitrage Zur schotteranalyse, *Schweizerische Mineralogische und Petrographische Mitteilungen*, 15, 39–14.

1. **Table 1 and Figures/Captions**

Table 1. Summary of Rock Height and Shape Parameters For Basalt Rocks at *InSight*

Location	Average Rock Height	10 Tallest Rocks	Height Short Axis %	Max Proj. Spher. (Ave./Range)	Dev. Comp
Exterior	6 cm	23-30 cm	78%	0.35/0.11-0.87	0.18/
Margin	4 cm	4-33 cm	91%	0.33/0.10-0.81	0.16/
Interior	1 cm	14-26 cm	97%	n/a	
Lonar Ejecta	n/a	n/a	n/a	0.72/0.11-1.0	0.53/
Exterior +10 cm	n/a	n/a	n/a	0.65/0.29-0.85	0.45/

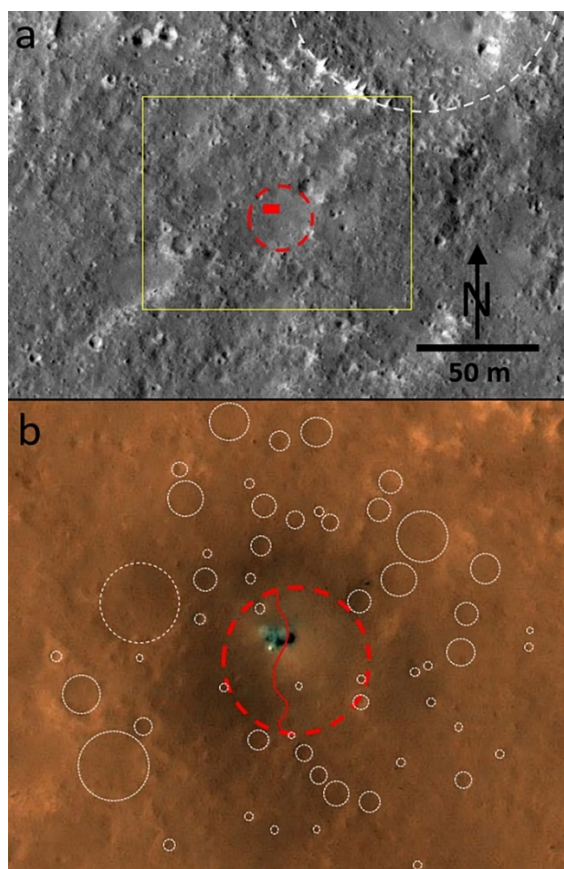


Figure 1. (a) The *InSight* lander (red box) in the 27 m-diameter *Homestead hollow* degraded impact crater (red dashed circle) in western Elysium Planitia, Mars (4.502°N , 135.623°E). The lander is 6 m measured across the solar panels, is in the northwestern quadrant of the hollow, and the lander workspace is to the south. Yellow box shows location of (b). Subframe of HiRISE color ESP_036761_1845 (0.25 m/pixel). (b) Color view of *InSight* lander in *Homestead hollow* (red dashed circle) and other hollows (white dotted circles) in the immediate vicinity. Red line cutting across the hollow is the boundary between occurrence of relatively few rocks to the east versus $\sim 3\text{X}$ more rocks in the region to the west dubbed “*Rocky Field*” (see Figure 2). Landing rockets removed

dust from the immediate surface and caused the bright zone and surrounding dark halo around the lander (Williams et al., 2020). Subframe of HiRISE color image ESP_061684_1845 (0.25 m/pixel). Modified from Fig. 1 in Grant et al. (2020).

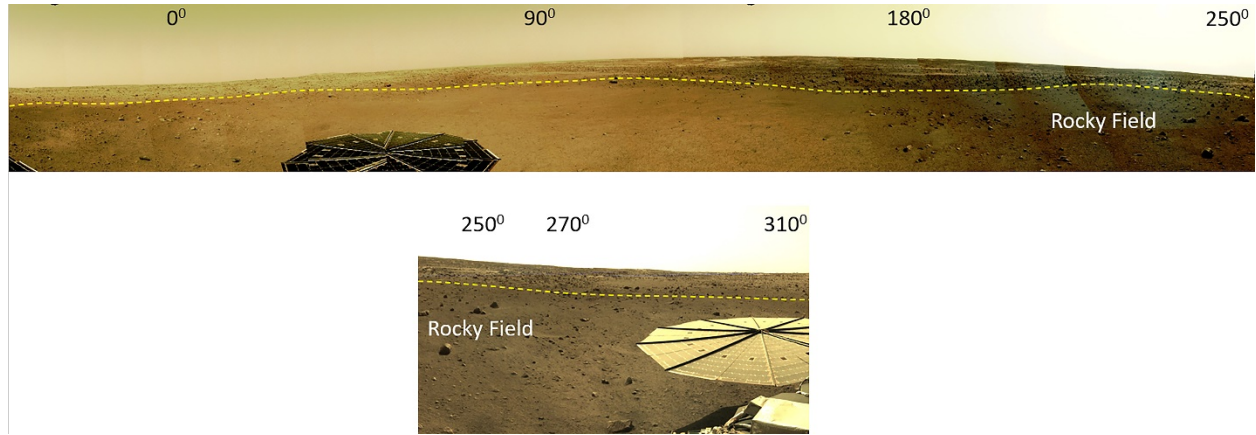


Figure 2. Mosaic covering approximately 290 degrees around the north, east and south side of lander in *Homestead hollow* (top) and mosaic covering approximately 70 degrees around the west side of the lander (bottom). Near- and mid-field coverage in the mosaics matches that shown in the orthomosaic/DEM in Figure 3 and enabled measurement of rocks within 10 m of the lander across a broad swath of the hollow interior, within ~1 meter of the margin (yellow dashed line) to the west to the north side of the hollow, and on the west/north near-rim within a few meters outside the hollow rim. For scale, the lander solar panels in both mosaics are 2.15 m in diameter. Rocky Field denotes the ~3X higher density of rocks on the west-northwest part of the hollow interior. Numbers refer to azimuth where 0° is true north. Mosaic D_LRGB_0014_RAS030100CYL_R__SCIPANQM1 (a) and IDC Mosaic D_LRGB_0119_RAD030100CYL_R__AUTOGENM3 (b). Small black areas around mosaic margins are gores in the image data.

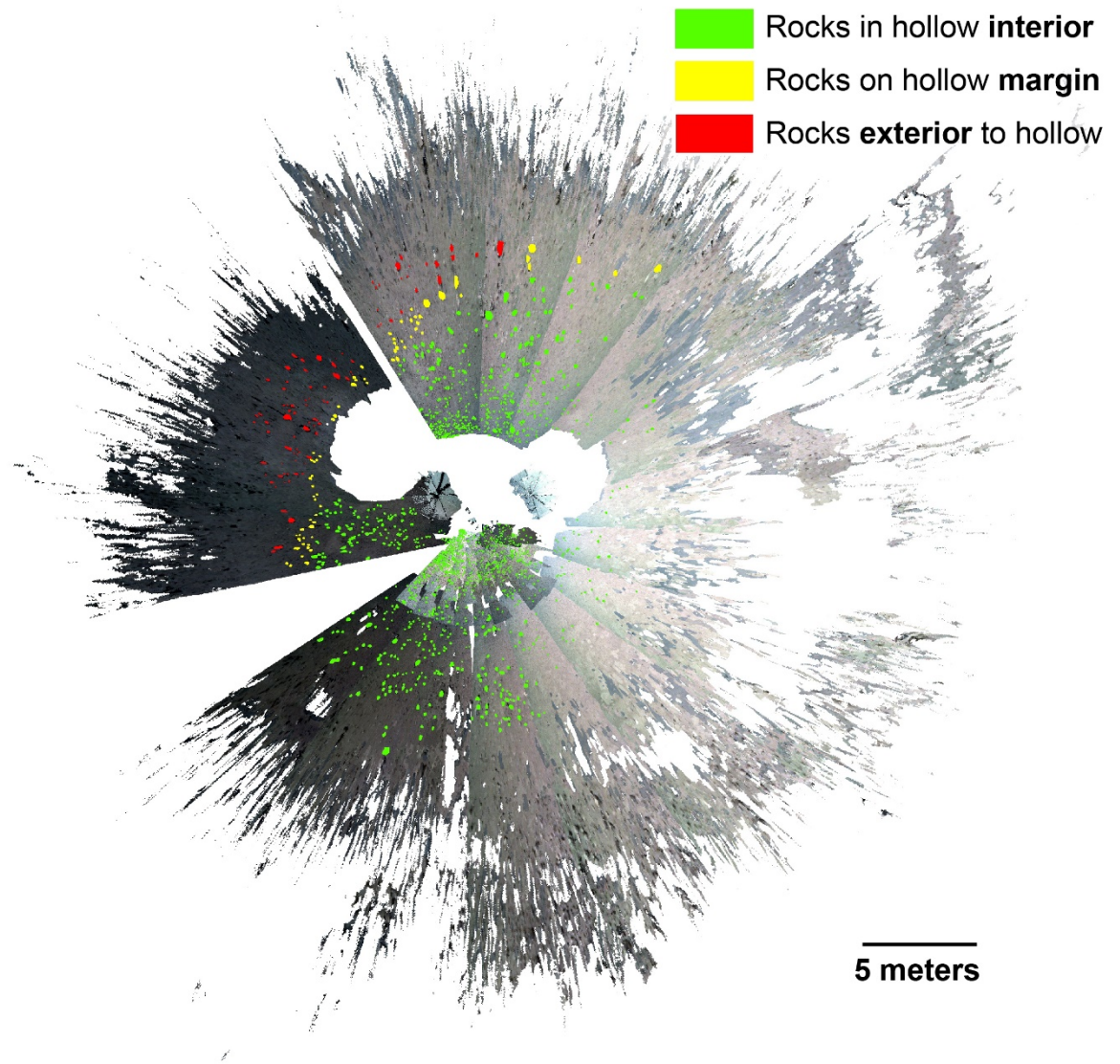


Figure 3. Image of the IDC orthomosaic coverage in and around *Homestead hollow* that covers much of the same area visible in the near- and mid-fields in Figure 2. The current study focuses on rocks within 10 m of the lander and included rocks across a broad swath of the hollow interior (green), within ~1 meter of the margin to the west of the north side of the hollow (yellow, see Figure 2), and outside of the hollow within a few meters of rim to the west and north of the lander (red).

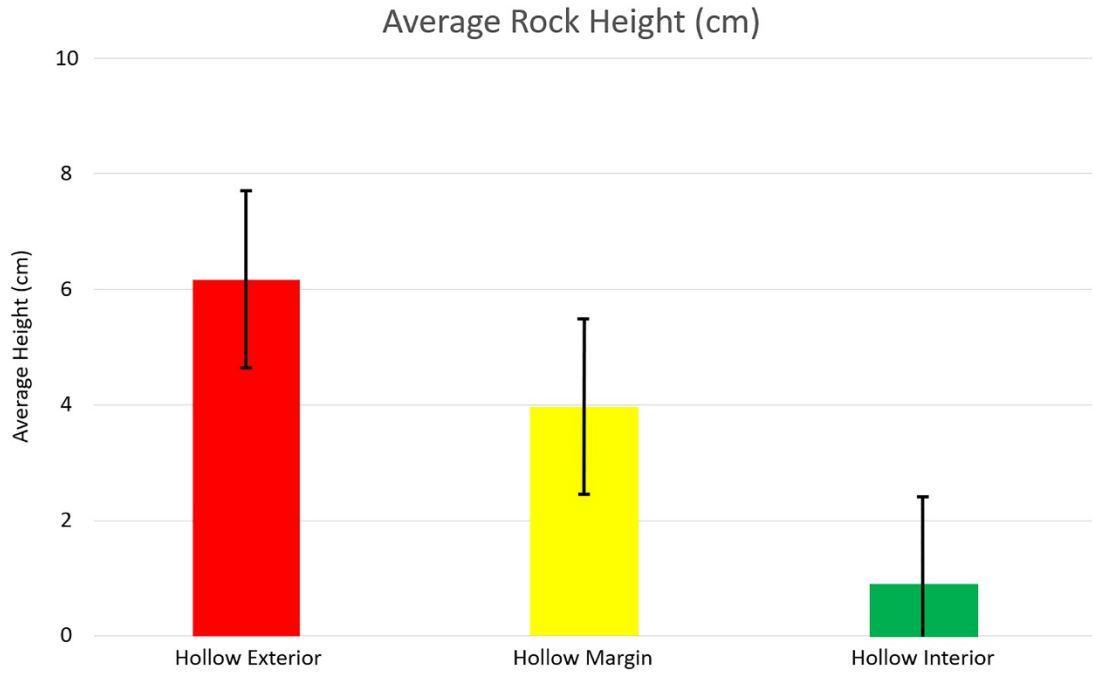


Figure 4. Average height of rocks around the exterior, margin, and interior of Homestead hollow are 6 cm, 4 cm, and 1 cm, respectively. All rocks measured in the DEM are included in the average and the standard error is indicated (standard deviation $N/\text{square root of } N$) that indicates the relative differences in rock height between the three areas are significant (especially between the exterior and interior). Because the rocks around the exterior and margin are more exposed based on their greater size and relative relief, their values are emphasized in consideration of the average amount of eolian stripping that has occurred outside the hollow (Golombek, Warner et al, 2020; Grant et al., 2020; Warner, Grant, et al., 2020) and how much rock fragments may remain embedded in the remnant ejecta.

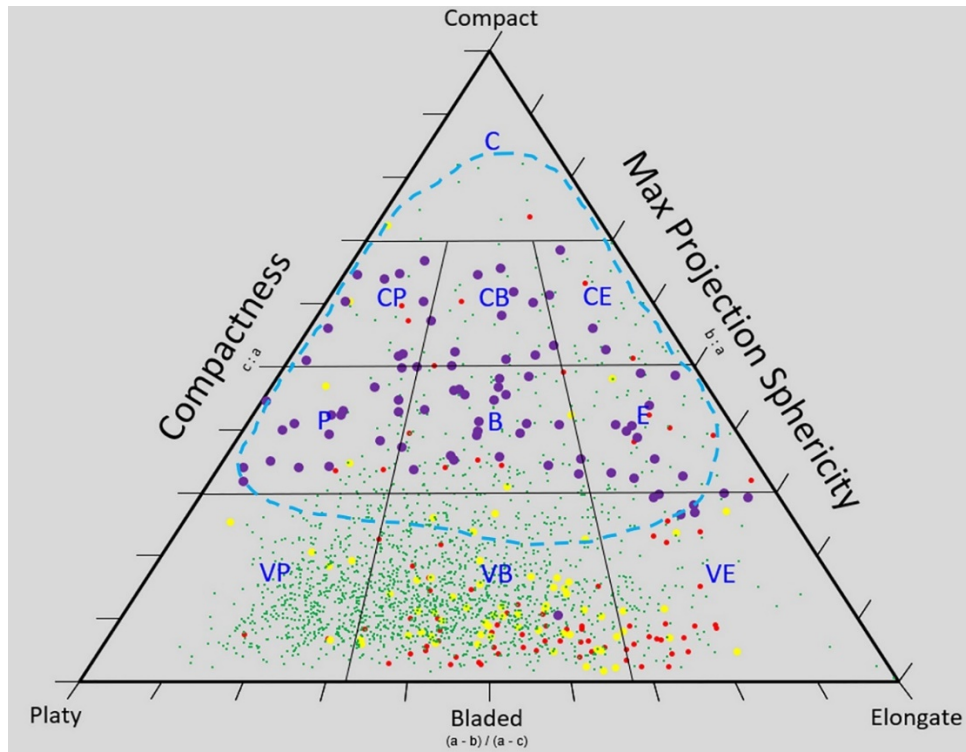


Figure 5. Form factor of basalt rocks in and around the *InSight* lander in *Homestead hollow*. The shape of *InSight* fragments within (green dots), around (yellow dots), and outside (red dots) the hollow plot as mostly platy, bladed, and elongate, whereas the blue dashed line indicates the data cloud for the vast majority of the basalt rocks in ejecta at Lunar crater (Kumar et al., 2014) that is similar to that for basalt rocks in other terrestrial environments (e.g., Ehlmann et al., 2008; Craddock and Golombek, 2016). Purple dots plot the shape of fragments outside the hollow when it is assumed that the rocks remain embedded 10 cm in the remnant ejecta deposit and are generally similar to the shape of basalt fragments defined in terrestrial studies if fully exposed. Field names with abbreviations are: C - compact, CP - compact platy, CB - compact bladed, CE - compact elongated, P - platy, B - bladed, E - elongate, VP - very platy, VB - very bladed, and VE - very elongated. Note that the extreme shapes of Lunar fragments (VP, VB, and VE) are fewer than other shapes.

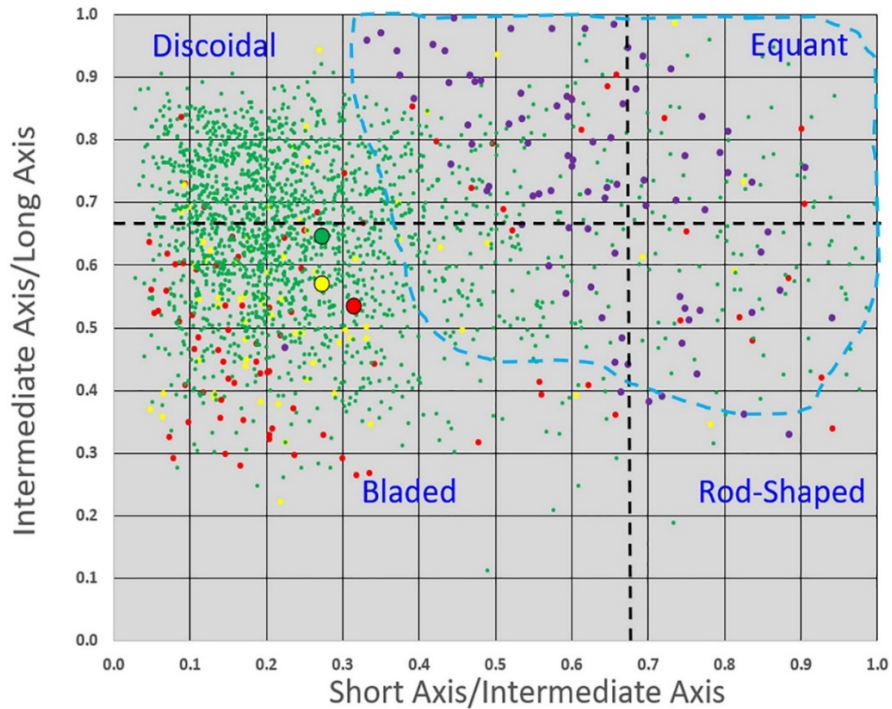


Figure 6. Plot of fragment shape as defined by the ratio of the intermediate to short axis versus the short to intermediate axis after Zingg (1935). There is significant scatter in the data, but the bulk of fragments inside the hollow (green dots) plot near the boundary between discoidal and bladed shapes, whereas fragments along the margin (yellow dots) and outside (red dots) are somewhat more bladed in shape. The large red, yellow, and green dots mark the average of the rocks on the exterior, margin, and interior of the hollow, respectively, and highlight the general similarity in rock shape in and around the hollow. The blue dashed line encompasses the data cloud for the vast majority of basalt ejecta fragments at Lonar crater (Kumar et al., 2014) that is similar to that for basalt rocks in other terrestrial environments (e.g., Ehlmann et al., 2008; Craddock and Golombek, 2016) and are mostly equant (34%) with lesser, but significant disc-, rod- (28%), and blade-shapes (10%). Purple dots are fragments outside the hollow when it is assumed that the rocks remain embedded 10 cm in the surface and are generally similar to the shape of basalt fragments noted in terrestrial studies.